

**People's Democratic Republic of Algeria**  
**Ministry of Higher Education and Scientific Research**  
**University M'Hamed BOUGARA – Boumerdes**



**Institute of Electrical and Electronic Engineering**  
**Department of Electronics**

Final Year Project Report Presented in Partial Fulfilment of  
the Requirements for the Degree of

**MASTER**

**In Control Engineering**

**Option: Control**

Title:

**Realization of a Semi-Automatic Test Bench  
for Induction Motor Characterization**

Presented by: - **Zenimi Nassim**  
- **Boulala Mohamed Aymen**

Supervisor: **Pr. Hamid Bentarzi**

Number ..... /2023

## **Acknowledgment**

We would like to express our sincere gratitude to our families for their unwavering support, encouragement, and understanding throughout the duration of this project. Their love, patience, and belief in our abilities have been invaluable, and we are truly grateful for their presence in our lives.

We extend our deepest appreciation to Mr. Bentarzi, our supervisor, for his guidance, expertise, and continuous encouragement throughout the project. His valuable insights, constructive feedback, and mentorship played a vital role in shaping the direction and success of our work. We are grateful for his dedication and support.

We would also like to thank Mr. Ouadi, who generously provided us with assistance, guidance, and valuable suggestions. His expertise and willingness to share his knowledge were instrumental in overcoming challenges and enhancing the quality of our project.

Furthermore, we extend our heartfelt thanks to the University of Boumerdes and the Institute of Electrical and Electronic Engineering for providing us with the necessary resources, facilities, and academic environment. The university's commitment to fostering excellence in education and research has greatly contributed to our personal and professional growth.

## **Dedication**

*To my exceptional family, especially my remarkable mother, I dedicate this thesis. Your unwavering support, love, and sacrifices have propelled me to this milestone. I am forever grateful for your belief in me.*

**Boulala Mohamed Aymen**

*I dedicate this work to my parents, who have always been there for me, supporting and guiding me. I am truly grateful for everything you have done and for believing in me. Your love and presence in my life mean the world to me.*

**Zenimi Nassim**

## **Abstract**

The efficient testing and characterization of induction motors play a crucial role in ensuring their optimal performance and reliability in various industrial applications. This project focuses on the development and implementation of a semi-automatic test bench for the characterization of induction motors. The objective is to create a reliable and user-friendly platform that allows for accurate measurement and analysis of motor parameters. The literature review provides a comprehensive overview of induction motors, covering their structure, functioning, equivalent circuit, power flow, and characteristics. Additionally, the review delves into NEMA classes, examining their implications for motor performance. The methods and measurement system section explores classical tests for induction motors, including the locked rotor test, no-load test, and DC test. Various measurement methods and signal conditioning techniques are discussed, encompassing voltage, current, speed, and torque measurements. The utilization of LabVIEW software and data acquisition devices is also examined in detail. The developed platform description and testing section presents the architecture and functionality of the semi-automatic test bench. It showcases a tab control interface with different tabs for various tests, including no-load test, blocked rotor test, DC test, and speed-torque analysis. The Parameters tab allows for comprehensive motor parameterization.

# Contents

Acknowledgment . . . . .	i
Dedication . . . . .	ii
Abstract . . . . .	iii
List of Figures . . . . .	vi
Introduction . . . . .	1
<b>1 Literature Review</b>	<b>3</b>
1.1 Introduction . . . . .	3
1.2 The structure of an induction motor . . . . .	3
1.2.1 Types of induction motors . . . . .	4
1.3 The functioning of induction motors . . . . .	5
1.4 Equivalent circuit of an induction motor . . . . .	6
1.4.1 IEEE recommended equivalent circuit of an induction motor . . . . .	7
1.5 Power flow and losses of an induction motor . . . . .	8
1.6 The capabilities and characteristics of an induction motor . . . . .	10
1.6.1 Torque-speed characteristics . . . . .	11
1.6.2 Power factor, Stator current and efficiency . . . . .	11
1.7 NEMA Classes . . . . .	12
1.7.1 Class A . . . . .	13
1.7.2 Class B . . . . .	13
1.7.3 Class C . . . . .	13
1.7.4 Class D . . . . .	14
1.8 Conclusion . . . . .	14
<b>2 Methods and Measurement System</b>	<b>15</b>
2.1 Introduction: . . . . .	15
2.2 Classical tests of induction motors . . . . .	15
2.2.1 Locked rotor test . . . . .	16
2.2.2 No-load test . . . . .	18
2.2.3 DC test . . . . .	20
2.3 Measurement methods and signal conditioning . . . . .	21
2.3.1 Voltage measurement . . . . .	22
2.3.2 Current Measurement . . . . .	25
2.3.3 Speed Measurement . . . . .	26
2.3.4 Torque Measurement . . . . .	28
2.4 LabVIEW and DAQ . . . . .	33

2.4.1	LabVIEW . . . . .	33
2.4.2	Data Acquisition Device . . . . .	40
2.5	Conclusion . . . . .	45
<b>3</b>	<b>Developed Platform Description and Testing</b>	<b>46</b>
3.1	Introduction . . . . .	46
3.2	Tab Control Interface . . . . .	48
3.2.1	Home tab . . . . .	48
3.2.2	No Load Test tab . . . . .	49
3.2.3	Blocked Rotor Test tab . . . . .	50
3.2.4	DC Test tab . . . . .	52
3.2.5	Speed-Torque tab . . . . .	52
3.2.6	The Parameters tab . . . . .	54
3.3	Conclusion . . . . .	55
<b>Conclusion</b>		<b>56</b>
	Bibliography . . . . .	56
	Appendix . . . . .	59

# List of Figures

1.1	Cage rotor construction. The stack of pre-punched laminations is shown on the left, with the copper or aluminum rotor bars and end-rings on the right. . . . .	4
1.2	Schematic diagram of wound rotor for induction motor, showing sliprings and brushes to provide connection to the external (stationary) 3-phase resistance. . . . .	5
1.3	Steinmetz model of an induction motor . . . . .	6
1.4	Precise equivalent circuit of the induction motor with rotor parameters referenced to the stator . . . . .	7
1.5	Approximate equivalent circuit of an induction motor . . . . .	8
1.6	Power flow diagram of an induction motor . . . . .	10
1.7	Torque-speed characteristic curve at different modes of operation. . . . .	11
1.8	IEEE-Recommended Equivalent Circuit. . . . .	12
2.1	Diagram of a locked rotor test . . . . .	16
2.2	simplified equivalent circuit at locked rotor test . . . . .	17
2.3	Diagram of the no-load test . . . . .	18
2.4	Graph of the applied voltage versus the input power . . . . .	19
2.5	simplified equivalent circuit under no-load test . . . . .	20
2.6	Diagram of an induction motor under DC test . . . . .	21
2.7	Voltage measurement part of the testing circuit . . . . .	22
2.8	Circuit illustrating a voltage divider . . . . .	23
2.9	2 <sup>nd</sup> Order Sallen-Key Low Pass Filter . . . . .	24
2.10	Voltage Sensor Module along with its corresponding circuit . . . . .	24
2.11	Current measurement part of the testing circuit . . . . .	25
2.12	Typical application of the ACS712T sensor . . . . .	25
2.13	Functional Block Diagram of the ACS712T sensor . . . . .	26
2.14	Speed measurement part of the testing circuit . . . . .	27
2.15	Picture of the M18 Retro-Reflective Sensor . . . . .	27
2.16	Internal Diagram of the M18 Sensor . . . . .	28
2.17	Torque measurement part of the testing circuit . . . . .	29
2.18	Strain Gauges arranged in a Wheatstone Bridge . . . . .	30
2.19	Internal Diagram and Basic Connections of the INA101 . . . . .	32
2.20	LabVIEW virtual instrument front panel. . . . .	34
2.21	LabVIEW virtual instrument block diagram. . . . .	35
2.22	An XY graph. . . . .	35
2.23	Waveform Graph. . . . .	36
2.24	Example of a Power and Frequency Estimator using the LabVIEW Electrical Power Toolkit . . . . .	39

2.25	Pinout of the NI USB-6009 . . . . .	41
2.26	Analog input measurement. . . . .	44
2.27	Configuration of the Task . . . . .	44
3.1	Nameplate of the used induction motor . . . . .	47
3.2	Nameplate of the used dynamo . . . . .	47
3.3	Home Tab during the No-Load Test . . . . .	48
3.4	Home Tab during the Blocked Rotor Test . . . . .	49
3.5	No Load Tab during the No Load Test . . . . .	50
3.6	Blocked Rotor Tab during the Blocked Rotor Test . . . . .	51
3.7	DC Tab during the DC Test . . . . .	52
3.8	Speed-Torque Tab . . . . .	53
3.9	Parameters Tab . . . . .	54



# Introduction

Induction motor testing plays a crucial role in various scenarios. Whether it is performed by factories aiming to validate their products before delivering them to end users, or by end users themselves seeking to assess the motor's condition prior to use or after prolonged operation.

Traditionally, the testing of induction motors relied on available techniques and devices. However, contemporary approaches employ an assortment of sensors and data acquisition devices, which greatly simplify the testing process for non-experts.

Users now only need to perform simple tasks, such as connecting cables or activating switches, while being guided by the Human User Interface in LabVIEW. The remainder of the testing procedure is automated by the test bench, employing the LabVIEW graphical programming language. This comprehensive system conducts the necessary calculations and data processing, and provides users with the final results and a range of motor parameters.

In this testing setup, an NI USB-6009 data acquisition device is employed. This device processes information gathered from speed, voltage, current, and torque sensors, and transfers the data to a computer for further analysis. The implementation of a test bench offers several advantages over traditional testing methods, including swifter processing, enhanced accuracy, improved reliability, and heightened stability.

Although substantial research has focused on online monitoring and parameter testing, the LabVIEW data acquisition approach remains relatively underexplored in the literature. This approach presents an affordable and readily accessible Human User Interface, requiring nothing more than a computer equipped with the LabVIEW software.

The first chapter provides an overview of the thesis and introduces the topic of induction motors. It starts with a general introduction, highlighting the importance and relevance of studying induction motors. It then proceeds to discuss the structure of an induction motor, including different types of induction motors. The functioning of induction motors is explained, along with the equivalent circuit model. Power flow, losses, and the capabilities and characteristics of induction motors are also covered. The chapter concludes by introducing NEMA Classes, which classify induction motors based on their operating characteristics.

In the second chapter, the focus is on the methods used to test and measure induction motors. It begins by discussing classical tests, including the locked rotor test, no-load test, and DC test, which are commonly performed to characterize induction motors. The chapter then delves into measurement methods and signal conditioning techniques for voltage, current, speed, and torque measurements. Additionally, it introduces LabVIEW, a software development environment, and Data Acquisition (DAQ) devices commonly used in motor testing and measurement.

The third chapter presents the developed platform for testing induction motors and provides a detailed description of its features. It starts with an introduction to the chapter and proceeds to explain the Tab Control Interface. Each tab within the interface is described, including the Home tab, No Load Test tab,

Blocked Rotor Test tab, DC Test tab, Speed-Torque tab, and Parameters tab. These tabs provide various functionalities and controls for conducting different tests and analyzing the performance of induction motors. The chapter concludes with an overview of the developed platform's capabilities and its potential for motor testing.

# Chapter 1

## Literature Review

### 1.1 Introduction

The electric motor, quite possibly one of humanity's most remarkable innovations, is a brilliant device that functions as an astute energy converter. It has the remarkable capability to generate kinetic energy through the utilization of a mere configuration comprising copper coils and steel laminations.[6]

This chapter aims to offer a comprehensive overview of induction motors, encompassing their diverse types and architectures. Additionally, it will delve into the principle behind their operation and shed light on how these motors ingeniously convert electrical energy into kinetic energy.

Furthermore, it will explore how these intricate devices can be represented through a simplified electrical circuit known as the equivalent circuit. Notably, the chapter will also highlight the noteworthy contribution of Steinmetz in the field of electricity, where he bridged the gap between the transformer-oriented approach and electric motors.

Lastly, this chapter will explain the power flow of induction motors and explore the different parameters that differentiate them from each other, including efficiency, speed-torque curve, power factors, and more. Additionally, it will discuss the various classes of induction motors, shedding light on how these classifications contribute to their distinct characteristics.

### 1.2 The structure of an induction motor

Induction motors are commonly used in many industrial and commercial applications because of their simplicity, reliability, and energy efficiency. The construction of an induction motor consists of two main parts: the stator and the rotor.[3]

The stator consists of three parts;

The stator frame, which is the outer part of the induction motor that provides protection to the inner parts of the motor and keeps the rotor centric with the stator. It is usually made up of fabricated steel or

die-cast.[3]

The stator core, which carries the alternating flux and reduces eddy current losses, it is made up of stamping stamped together which form the stator core that is housed inside the previously discussed stator frame. It is usually made up of silicon steel stamping.[3]

## 1.2.1 Types of induction motors

There are two types of induction motors

**Squirrel cage induction motor:** Its rotor is cylindrical with slots on its periphery, these slots are a little skewed which helps prevent problems like magnetic locking of the stator and rotor teeth which in turn makes the working of the motor smoother and quieter.[7, 13]

The squirrel cage rotor is usually made up of aluminum, brass or copper bars and the rotor conductors are perpetually shorted by aluminum or copper rings called end rings. The winding of a squirrel cage rotor is symmetrical, it is widely used in industry due to the absence of slip ring and brushes which makes its construction very simple and sturdy.[13]

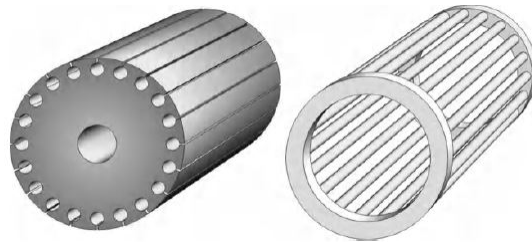


*Figure 1.1:* Cage rotor construction. The stack of pre-punched laminations is shown on the left, with the copper or aluminum rotor bars and end-rings on the right.

**Slip Ring or Wound Rotor:** In this type motor the rotor is wound for the same number of poles as that of the stator, it has less slots and turns per phase of a heavier conductor.[13]

The rotor has a set of windings that are connected to slip rings which allow an external resistance to be connected to the rotor windings, this resistance makes controlling the motor possible by increasing the resistance we can increase the torque and decrease speed and vice-versa.[13]

The slip ring motor can handle high starting torque loads but is less efficient than other types of induction motors because the slip rings and external resistance present in the rotor circuit causes power losses and decrease the overall efficiency of the motor and the motor usually requires higher maintenance

and is prone to various problems.[13]

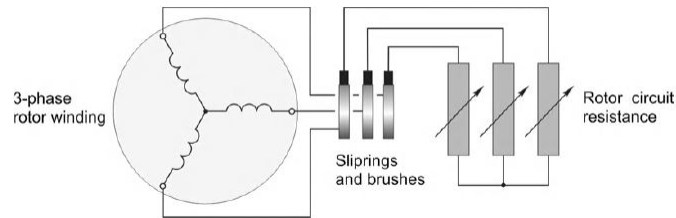


Figure 1.2: Schematic diagram of wound rotor for induction motor, showing sliprings and brushes to provide connection to the external (stationary) 3-phase resistance.

### 1.3 The functioning of induction motors

When the A.C power source is turned on, the alternating magnetic field in the stator induces a magnetic field in the rotor. The magnetic field in the rotor creates an electromotive force in the conductive bars.[5, 6, 13]

The EMF in the rotor creates a current in the bars that flows in a direction perpendicular to the magnetic field.[13]

The interaction between the magnetic field in the stator and the current in the rotor creates a force that causes the rotor to turn. As the rotor turns, the conductive bars cut through the magnetic field in the stator, which creates a voltage in the rotor.[13]

This voltage creates a current in the rotor, which in turn creates a magnetic field that opposes the magnetic field in the stator. This opposition to the stator's magnetic field is what allows the rotor to turn.[13]

The synchronous speed, denoted as  $N_s$  and measured in revolutions per minute, can be represented by a universal equation that defines the velocity of the field.[13, 6]

$$N_s = \frac{120f}{p} \quad (1.1)$$

Where  $f$  is the stator voltage frequency and  $p$  the number of poles

The slip speed is the difference in velocity between the rotor and the field, and it is expressed as  $N_s - N$ , where  $N$  is the speed of the rotor and  $N_s$  is the synchronous speed of the field, usually measured in revolutions per minute. The slip can be defined as follows:[13, 5]

$$s = \frac{(N_s - N)}{N_s} \quad (1.2)$$

The speed of the relative movement between the rotor and field determines both the frequency and

magnitude of the rotor induced voltage, which are respectively expressed as,[13]

$$f_r = sf_s \quad (1.3)$$

$$E_r = 4.44nsf_s\phi_{max} \quad (1.4)$$

## 1.4 Equivalent circuit of an induction motor

The induction motor bears similarities to the synchronous motors in some regards, while it shares similarities with the transformer in other aspects. The polyphase induction machine's most commonly employed circuit model was established by Charles Steinmetz.[14, 12]

Steinmetz adopted a transformer-oriented approach in his development of the model, which has proven to be highly valuable in comprehending the induction machine's properties. Nevertheless, when the model impedances are determined through laboratory measurements, the model's numerical data is not particularly precise regarding the machine's performance.[14, 12]

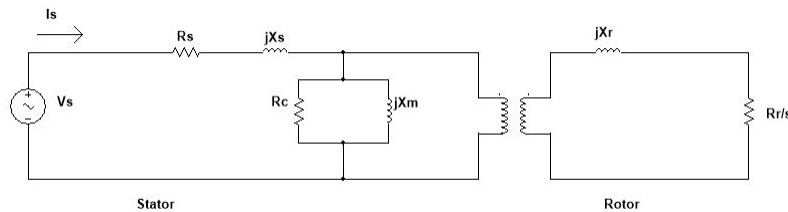


Figure 1.3: Steinmetz model of an induction motor

In the previous figure,[14, 12]

$R_s$  is the winding resistance of the stator.

$X_s$  is the inductance of the stator winding.

$R_c$  is the core loss component.

$X_M$  is the magnetizing reactance of the winding.

$\frac{R_r}{s}$  is the power of the rotor, which includes output mechanical power and copper loss of rotor.

The previous circuit could be simplified by referencing the rotor's parameters to the stator's, assuming both have an equivalent number of turns.

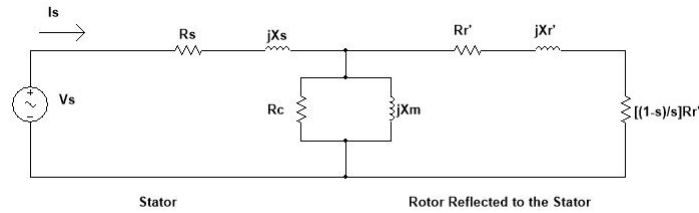


Figure 1.4: Precise equivalent circuit of the induction motor with rotor parameters referred to the stator

Parameters are the same as the previous circuit except for, [14, 12]

$R_2'$  which is the rotor winding resistance with referred to stator winding.

$X_r'$  which is the rotor winding inductance with referred to stator winding.

$\frac{R_r(1-s)}{s}$  which is the resistance which shows the power which is converted to mechanical power output or useful power. The power dissipated in that resistor is the useful power output or shaft power.

### 1.4.1 IEEE recommended equivalent circuit of an induction motor

The IEEE (Institute of Electrical and Electronics Engineers) has provided a recommended equivalent circuit for modeling an induction motor. This equivalent circuit represents the electrical characteristics and parameters of the motor and allows for the analysis of its performance and behavior.

The IEEE recommended equivalent circuit includes

The stator winding resistance ( $R_s$ ): which represents the resistance of the stator winding.

The stator winding reactance ( $X_s$ ): which accounts for the leakage flux in the stator winding.

The rotor resistance referred to the stator ( $R_r'$ ) which represents the resistance of the rotor winding as seen from the stator side.

The rotor reactance referred to the stator ( $X_r'$ ): Accounts for the leakage flux in the rotor winding as seen from the stator side.

The magnetizing reactance ( $X_m$ ): which represents the reactance associated with the magnetizing current, which establishes the magnetic field in the motor. [2]

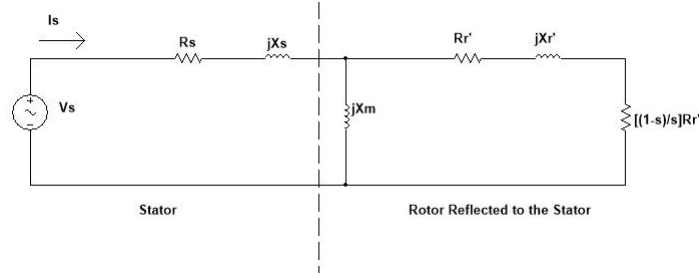


Figure 1.5: Approximate equivalent circuit of an induction motor

## 1.5 Power flow and losses of an induction motor

When an electrical input is given to the stator, it experiences losses due to the presence of copper and core components. The remaining power then proceeds across the air gap to reach the rotor. Once it reaches the rotor, there are losses associated with both the copper and iron components. However, these losses are typically small when compared to those of the stator's iron loss. Thus, they are generally grouped with the mechanical losses and collectively referred to as rotational losses.[14]

Despite the occurrence of these losses, the remaining power is converted into mechanical power. Nonetheless, some mechanical losses arise as well, leaving the final output power available as mechanical power. Overall, this process involves several stages and mechanisms, including the transformation of electrical input power into mechanical output power. Furthermore, it highlights the importance of mitigating losses wherever possible to maximize efficiency and optimize performance.[14, 5]

For a balanced 3-phase induction motor, the power input is[9]

$$P_{in} = 3V_1 I_1 \cos(\varnothing) \quad (1.5)$$

Where  $\varnothing$  is the input power factor, and

$$I_1 = \frac{V_1}{Z_{eq}} \quad (1.6)$$

Where,

$$Z_{eq} = |R_s + jX_s| + \left[ \left( \frac{R_r}{s} + jX_r \right) // R_C // jX_m \right]$$

$$Z_{eq} = R_s + jX_s + \frac{1}{G_C - jB_M + \frac{1}{\left| \frac{R_r}{s} + jX_r \right|}} \quad (1.7)$$

And,

$$I_2 = \frac{E_2}{\left| \frac{R_r}{s} + jX_r \right|} \quad (1.8)$$



Therefore, it is possible to determine the losses associated with the stator's copper components, as well as the losses due to the core and copper components in the rotor.

Stator Copper Loss is [9]

$$P_{cu1} = 3I_1^2 R_1 \quad (1.9)$$

Core losses are

$$P_C = 3E_1^2 G_C \quad (1.10)$$

As a result, it is possible to calculate the power that crosses the air gap as,

$$P_{ag} = P_{in} - P_{cu1} - P_C \quad (1.11)$$

By analyzing the equivalent circuit of the rotor, it becomes apparent that the resistance  $R_2/s$  is the sole element capable of consuming the power that crosses the air gap. Hence, it can be concluded that:[9]

$$P_{ag} = \frac{3I_2^2 R_r}{S} \quad (1.12)$$

However, the actual resistive losses occurring in the rotor winding are:

$$P_{cu2} = 3I_2^2 R_r = sP_{ag} \quad (1.13)$$

Therefore, the mechanical power that is produced can be calculated as:

$$P_{conv} = P_{ag} - P_{cu2} = \frac{3I_2^2 R_r}{S} - 3I_2^2 R_r = 3I_2^2 R_r \left( \frac{1}{S} - 1 \right) \quad (1.14)$$

$$P_{conv} = 3I_2^2 R_r \frac{(1-S)}{S} = (1-S)P_{ag} \quad (1.15)$$

Using the equation 1.8 to replace variables in equation 1.15 results in.[9, 8]

$$P_{conv} = \frac{3R_r E_2^2 (1-S)}{S \left( \left| \frac{R_r}{S} + jX_r \right| \right)^2} \quad (1.16)$$

Ultimately, the power produced through mechanical means can be determined by.

$$P_{out} = P_{conv} - P_{rot} \quad (1.17)$$

Where  $P_{rot}$  is the mechanical rotational losses in the machine.

The torque produced,  $T_d$ , can be acquired by utilizing the following relations.

$$T_d = \frac{P_{conv}}{\omega_m} = \frac{3I_r^2 R_r}{s\omega_m} \quad (1.18)$$

$$\omega_m = (1 - S)\omega_s \quad (1.19)$$

Here,  $\omega_m$  represents the actual mechanical speed of the device, whereas  $\omega_s$  refers to its synchronous mechanical speed.

$$\omega_s = \frac{4\pi f}{p} \quad (1.20)$$

By replacing the variables in equation 1.18 with those from equation 1.19, we obtain.

$$T_d = \frac{P_{conv}}{(1 - S)\omega_s} = \frac{3I_2^2 R_r}{s\omega_s} = \frac{P_{ag}}{\omega_s} \quad (1.21)$$

Likewise, we can determine the output torque,  $T_L$ , as.

$$T_L = \frac{P_{out}}{\omega_m} \quad (1.22)$$

The torque,  $T_L$ , that is accessible at the shaft is slightly lower than  $T_m$  because of the torque that is necessary to overcome windage and friction losses. Nonetheless, in most computations, we disregard this minor difference.[9, 8]

The losses in an induction motor can be resumed in the following figure.[9]

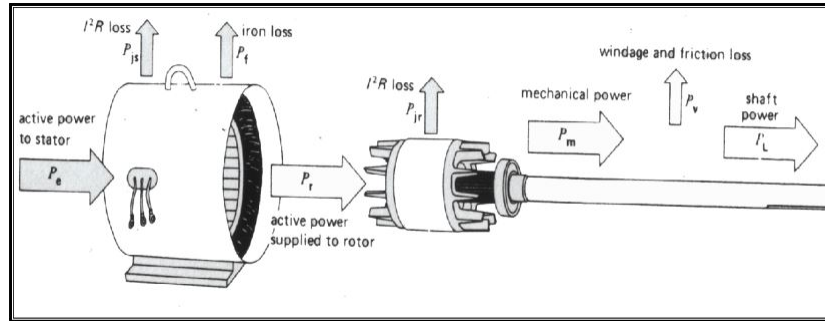


Figure 1.6: Power flow diagram of an induction motor

## 1.6 The capabilities and characteristics of an induction motor

Studying the performance characteristics of a machine, such as torque-speed relationship, efficiency, power factor, current, starting torque, and maximum torque, is crucial as it aids in determining the most suitable machine for a critical application.[6]

## 1.6.1 Torque-speed characteristics

The torque-speed characteristic illustrates how the developed torque of a machine is related to its mechanical speed and provides essential information, such as the pullout torque and starting torque of the machine.[13]

A torque-speed curve can be graphed for speeds that are either above or below the normal range of the motor, depicting the maximum and starting torque and various modes of operation.[13]

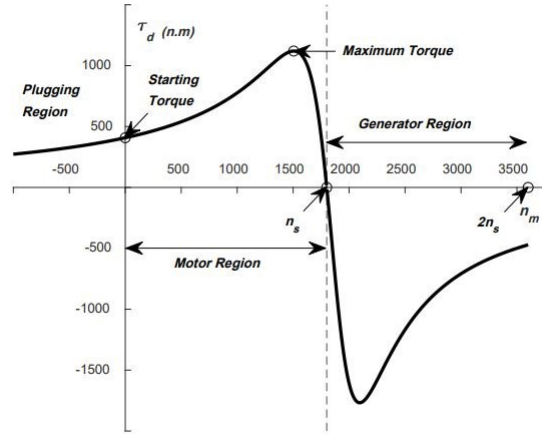


Figure 1.7: Torque-speed characteristic curve at different modes of operation.

To derive an expression for the maximum developed torque, the equation 1.24 needs to be differentiated with respect to slip  $s$  and equated to zero, thereby obtaining the condition for maximum torque.[9]

$$\frac{R_2}{S_{Tmax}} = \sqrt{R_{th}^2 + (X_{th} + X_2)^2} \quad (1.23)$$

The slip at maximum torque is.[9]

$$S_{Tmax} = \frac{R_2}{\sqrt{R_{th}^2 + (X_{th} + X_2)^2}} \quad (1.24)$$

As  $s=1$  at starting, the expression of starting torque is.[9, 1]

$$T_{dstart} = \frac{3V_{th}^2 R_2}{((R_{th} + \frac{R_2}{s})^2 + (X_{th} + X_2)^2) \omega_s} \quad (1.25)$$

## 1.6.2 Power factor, Stator current and efficiency

Using the following equivalent circuit,

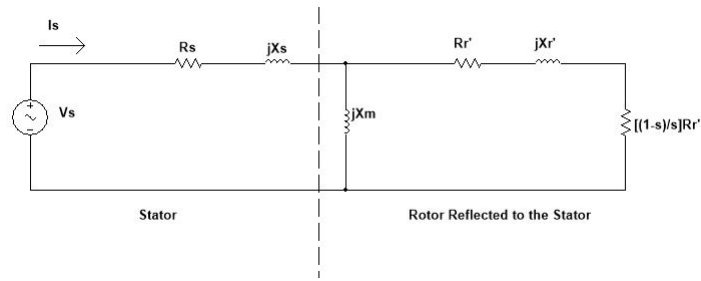


Figure 1.8: IEEE-Recommended Equivalent Circuit.

From Fig 1.8 the input impedance is[9, 13, 6]

$$\begin{aligned}
 Z_{eq} &= |R_s + jX_s| + \left[ \left( \frac{R_r}{s} + jX_r \right) // jX_m \right] \\
 &= |R_s + jX_s| + \frac{|jX_m(\frac{R_r}{s} + jX_r)|}{|(\frac{R_r}{s} + j(X_m + X_r))|} \\
 &= |Z_1| \angle \phi
 \end{aligned} \tag{1.26}$$

Hence, by using the input power factor, it is possible to calculate the stator current.[9, 13, 6]

$$PF = \cos(\phi) \tag{1.27}$$

The efficiency of the induction motor is.[9, 13, 6]

$$\eta = \frac{P_{out}}{P_{in}} \tag{1.28}$$

Induction motors possess another type of efficiency known as internal or ideal efficiency, which can be expressed as follows.[9, 13, 6]

$$\eta_{internal} = \frac{P_{com}}{P_{ag}} = (1 - s) \tag{1.29}$$

## 1.7 NEMA Classes

The squirrel-cage induction motors have been categorized into different types by the National Electrical Manufacturers Association (NEMA) through the use of letter designations A, B, C, and D. Each letter designation is carefully assigned to fulfill the particular requirements of a specific application.[1]

### **1.7.1 Class A**

Standard motors, known as Class A motors, are most appropriate for applications requiring a consistent speed.[1, 4]

These motors possess substantial rotor bars, leading to a relatively high starting current; however, their starting torque remains reasonable. Notably, these motors exhibit a remarkable level of torque near their rated RPM, owing to their large rotor bars that help maintain the rotor's full load speed in close proximity to the synchronous speed.[1, 4]

Consequently, these motors are capable of maintaining a nearly constant speed under various loads. During startup, the current drawn by these motors can range from 5 to 7 times the rated current, while their full load slip remains below 5% due to the rotor's low resistance.[1, 4]

Class A motors find common application in fans, blowers, centrifugal pumps, and machine tools.[1]

### **1.7.2 Class B**

Class B motors are versatile motors designed for general use and are activated by their specified voltage. They possess a higher resistance in their rotor compared to Class A motors.[1]

It's important to note that the rotor conductors are positioned deeper within the slots in comparison to Class A motors. As a result, the rotor reactance of Class B motors is greater than that of Class A motors. This enhanced rotor reactance leads to an increased starting torque, which in turn causes the starting current to be 4.5 to 5.5 times higher than the full-load current.[1]

Class B motors are typically constructed from low-cost cast aluminium and can be employed for the same applications as Class A motors.[1, 4]

### **1.7.3 Class C**

Class C motors exhibit higher starting torque and slip in comparison to Class B motors. They are equipped with a double-cage rotor and specifically designed for initiating operation at full voltage.[1]

The starting current of Class C motors is restricted to a range of 3.5 to 5 times the full load current. This limitation is implemented due to the presence of a high-resistance rotor. The starting torque of Class C motors ranges from 200% to 275% of the full load torque. These motors typically utilize copper or brass bars, which are prone to cracking due to their specific shape and the characteristics of the metal employed.[1, 4]

These motors find application in scenarios demanding substantial starting torque, including crushers, woodworking equipment, and conveyor systems.[1]

## **1.7.4 Class D**

Class D motors are utilized in situations where there is a need for exceptionally strong rotational force. These motors can effectively operate heavy loads without generating substantial heat. They possess the ability to produce a starting torque that is 250% to 300% higher than their initial torque output.[1, 4]

This increased torque is achieved by incorporating high-resistance alloys in the motor bars and reducing the cross-sectional area of the bars, resulting in higher rotor resistance. During startup, the current drawn by these motors ranges from 3 to 8 times the rated current. However, their efficiency is notably lower compared to motors belonging to other classes.[1, 4]

Typical applications for Class D motors include bulldozers, punch presses, laundry equipment, and shearing machines.[1, 4]

## **1.8 Conclusion**

In conclusion, Chapter 1 provided an overview of the fundamental concepts related to induction motors. We explored the structure of an induction motor and discussed different types of induction motors commonly used in various applications. The functioning of induction motors was explained, highlighting the principles of electromagnetic induction and the interaction between the stator and rotor. Additionally, we introduced the equivalent circuit of an induction motor, considering both the simplified and approximate models.

The chapter also touched upon power flow, losses, and the capabilities of induction motors, including torque-speed characteristics, power factor, stator current, and efficiency. Understanding these foundational concepts is crucial for further exploration in the subsequent chapters, where we will delve into specific methods, measurements, and testing techniques for induction motors.

# Chapter 2

## Methods and Measurement System

### 2.1 Introduction:

In order to comprehensively study and analyze induction motors, it is essential to employ appropriate methods and measurement systems. This chapter focuses on the methodologies and techniques utilized in the testing and measurement of induction motors. Accurate and reliable measurements enable researchers and engineers to obtain valuable data, leading to a deeper understanding of motor performance, efficiency, and characteristics.

The first section will focus on classical tests conducted on induction motors. These tests, including the locked rotor test, no-load test, and DC test, provide essential information regarding motor behavior under different operating conditions. The locked rotor test allows for the evaluation of starting characteristics, including starting current and torque. The no-load test helps determine parameters such as core losses and rotational losses when the motor operates without a load. The DC test enables the measurement of resistance and inductance parameters, providing valuable data for further analysis.

Accurate measurement of electrical quantities is crucial in understanding the intricate workings of induction motors. The second section will explore the measurement methods and signal conditioning techniques employed during motor testing. It covers various techniques for voltage measurement, including direct measurement and the use of potential transformers for higher voltage levels.

Current measurement methods, such as current transformers and current shunts, are discussed to capture the magnitude of electric current flowing through the motor. Additionally, the section delves into speed measurement methods, critical for analyzing motor performance and identifying operational characteristics. Finally, torque measurement techniques are explored, as torque is a fundamental parameter directly affecting motor performance and efficiency.

### 2.2 Classical tests of induction motors

There are three primary methods utilized to determine the parameters of an induction motor. The first is the locked rotor test, where the rotor is immobilized and low three-phase voltages are applied to the stator to circulate rated stator currents. This test is similar to a short circuit test of a transformer and is

used to obtain values for the rotor resistance and the rotor reactance.[10]

The second method is the DC test, where the rotor is stationary and a DC voltage is applied to measure the stator phase resistance based on the resulting current. The DC test is used to calculate the resistance of the stator.[14, 1]

Lastly, the no-load test involves driving the induction motor at synchronous speed using another motor, and then applying rated voltage at rated frequency to the stator while measuring the input power per phase. This test is used to determine the values of the core resistance and the magnetizing reactance, and is equivalent to the open circuit test of a transformer.[2]

## 2.2.1 Locked rotor test

The locked rotor test is a crucial method for gathering information about leakage impedances needed for the equivalent circuit, breakdown torque, and motor circle diagram. These details ensure a safe margin for motor overload capacity and account for voltage variations. Neglecting to perform this test correctly can potentially result in severe motor damage.[2, 9]

During the locked rotor test, the shaft of the motor is connected so that it cannot move and the rotor winding is short circuited, and the stator is supplied with a low voltage using a 3-phase auto-transformer to prevent excessive currents. The test is conducted under the same conditions of rotor current and frequency that will be encountered during normal operation. As per IEEE (Institute of Electrical and Electronics Engineers) recommendation, the frequency used is typically set at 25% of the rated frequency. This is because the rotor's effective resistance and leakage inductance may vary at reduced frequency compared to their values at the rated frequency.[2, 9]

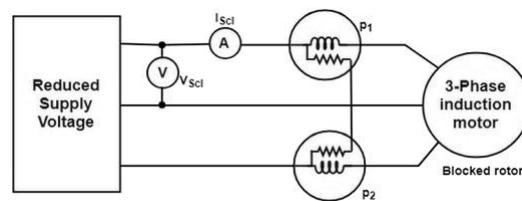


Figure 2.1: Diagram of a locked rotor test

The procedures to successfully do a locked rotor test are.[9, 2, 1, 13, 15]

1. Securing the induction motor's rotor shaft to the stationary disc using the supplied screws and ensuring that the rotor shaft is firmly secured in place.
2. Gradually raising the voltage of the three-phase stator from zero utilizing an auto-transformer.
3. Ceasing the process when the induction motor's stator reaches its rated current level.



4. Documenting pertinent measurements from the power analyzer.
5. Gradually reducing the voltage of the auto-transformer back to zero.

6. If the blocked rotor test needs to be conducted at input voltage frequencies other than the standard power frequency (50 Hz), employing a 'Variable Voltage Variable Frequency' (V.V.V.F) source instead of an auto-transformer.

From the readings of the devices present in the diagram of Fig 2.11 we can determine the following parameters.[9, 2]

We obtain the total power input on short-circuits from the readings of the two watt-meters.

$$P_{BR} = P_1 + P_2 \quad (2.1)$$

We obtain  $I_{sc1}$  ,the line current on short-circuit from the reading of the ammeter.

We obtain  $V_{sc1}$  ,the line voltage on the short circuit which can be used to obtain  $\therefore P_{BR}$

$$\therefore P_{BR} = \sqrt{3}V_{sc1} \text{Cos}(\varnothing_{sc})I_{sc} \quad (2.2)$$

Here  $\varnothing_{sc}$  is the power factor on short circuit.

Using the previous values, we can find the following.[9, 2]

$$R_{BR} = \frac{P_{BR}}{3I_{scp}^2} \quad (2.3)$$

Here  $R_{BR}$  is the equivalent resistance of the motor referred to the stator.

$$Z_{BR} = \frac{V_{scp}}{I_{scp}} \quad (2.4)$$

Here  $Z_{BR}$  is the equivalent impedance of the motor referred to the stator.[9, 2]

$$X_{BR} = \sqrt{Z_{BR}^2 - R_{BR}^2} \quad (2.5)$$

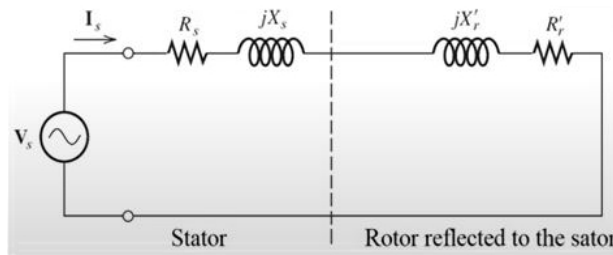


Figure 2.2: simplified equivalent circuit at locked rotor test

## 2.2.2 No-load test

The no-load test for a 3-phase induction motor is conducted while the motor is running without any load, and it provides information about the magnitude of constant losses that occur in the motor.[13] The setup for the no-load test is depicted in the Fig 2.13

The motor is started in the usual manner and allowed to run unloaded from the normal voltage mains. Suitable instruments are connected between the supply mains and motor terminals to measure power, line current, and line voltage.[13, 2]

Two single-phase watt meters are utilized for power and power factor measurement. As the motor is running without any load, the power factor of the motor is typically low, usually less than 0.5, causing one of the watt meters to display a negative reading. The total power consumed by the motor is the difference between the readings of the two watt-meters.[13, 2]

The signs of readings are recorded at various applied voltage values, and a curve is plotted against power and input voltage. From this curve, windage and friction losses can be determined.[13, 2]

As the motor is not loaded during the no-load test, the input power absorbed by the motor is utilized solely to account for losses. These losses occur in the iron core of both the stator and the rotor, and are known as core losses. A small amount of copper loss also occurs in the stator winding, but this can be neglected since the stator current is minimal.[13, 2]

Hence, the total power consumed during the no-load test is the sum of the rotor iron loss, stator iron loss, copper loss in the stator, and friction and windage loss. The readings taken at normal voltage and rated frequency are used to determine the fixed core losses.[13, 2]

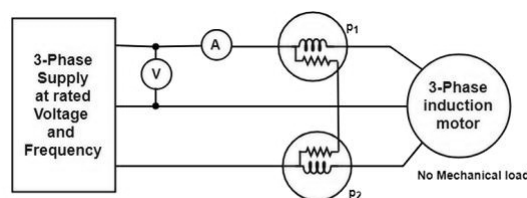


Figure 2.3: Diagram of the no-load test

The procedures followed to execute a no-load test on an induction motor are.[2, 9, 6, 13, 15]

1. Removing or disconnecting any mechanical load that is connected to the induction motor.
2. Slowly applying a three-phase voltage across the motor stator terminals using an auto-transformer.
3. As the stator voltage is gradually increased and the machine speeds up, ensuring that the voltage is applied in such a way that the machine does not accelerate too rapidly.

4. Setting the stator voltage to its rated value by making appropriate adjustments.
5. Note down no-load quantities such as  $V_{nl}$ ,  $I_{nl}$ ,  $P_{nl}$ .
6. Gradually reducing the stator voltage to zero and disconnecting the power supply.

The steps to determine the individual losses from a no-load test of an induction motor are as follows.

Reading  $P_o$  the power by the two watt-meters.[9]

Determining  $P_{scu}$  the copper losses in the stator.

$$P_{scu} = 3I_o^2R_s \quad (2.6)$$

Where  $I_o$  represents the no-load current measured by an ammeter at the normal voltage and rated frequency of the supply,  $R_s$  represents the stator winding resistance, and V per phase represents the applied voltage. The total constant losses  $P_{loss}$  is defined by.[9]

$$P_{loss} = P_o - 3I_o^2R_s \quad (2.7)$$

To determine the friction and windage losses, extend the curve plotted between the applied voltage and input power until it intersects the vertical axis.

The point of intersection represents the zero applied voltage. At zero applied voltage, the core losses and stator copper losses are also zero. Hence, the power input at no load and zero applied voltage represents the windage and friction losses.[9]

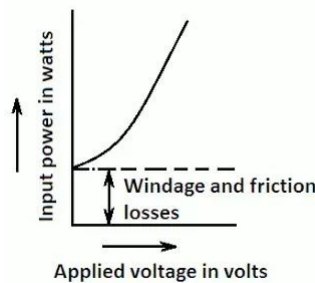


Figure 2.4: Graph of the applied voltage versus the input power

We have.

The no-load power factor which is defined as.[13]

$$\text{Cos}(\varnothing_o) = \frac{P_o}{3I_oV} \quad (2.8)$$

The no-load Impedance which is defined as.

$$Z_{NL} = \frac{V_{PH,NL}}{I_{PH,NL}} \quad (2.9)$$

The no-load resistance which is defined as.[13]

$$R_{NL} = \frac{V_{PH,NL}}{I_{PH,NL}^2} \quad (2.10)$$

The no-load reactance which is defined as.[13, 9]

$$X_{NL} = \sqrt{Z_{NL}^2 - R_{NL}^2} \quad (2.11)$$

simplified equivalent circuit under no-load test.

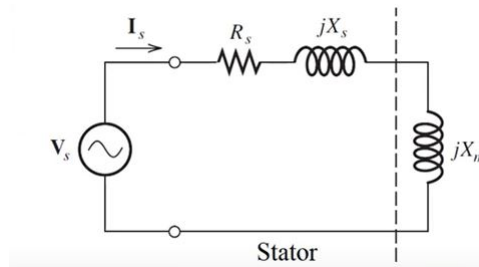


Figure 2.5: simplified equivalent circuit under no-load test

### 2.2.3 DC test

In the DC test of a 3-phase induction motor, a DC voltage is applied to the stator windings. Since the current is DC, there is no induced voltage in the rotor circuit, resulting in no rotor current. Additionally, the reactance of the motor is negligible at DC, meaning that the only factor limiting current in the motor is the stator resistance. This allows for the determination of the stator resistance during the DC test.[1, 13]

One of the primary objectives of the DC test is to ascertain the motor's winding resistance. This is achieved by administering a known DC voltage to the stator windings and gauging the resulting current, which enables the calculation of the winding resistance using Ohm's law. Winding resistance is a critical parameter that significantly impacts motor efficiency and performance.[1, 13]

Hence, precise measurement of winding resistance is imperative for motor performance analysis, protection, and control.[13]

Another noteworthy parameter evaluated during the DC test is the no-load current, which refers to the current drawn by the motor when it is devoid of any mechanical load. By measuring the no-load current at different voltages, it is possible to deduce the magnetizing current - the current necessary for establishing the motor's magnetic field. The magnetizing current is a crucial parameter used in motor

design and efficiency calculations.[3, 15]

Furthermore, the DC test can be employed to assess other motor characteristics, including core losses, stray losses, and iron losses. Core losses are incurred in the motor’s iron core due to hysteresis and eddy current losses. Stray losses arise from factors like leakage flux, while iron losses occur in the iron core due to diverse factors such as hysteresis, eddy currents, and magnetic aging.[1, 13]

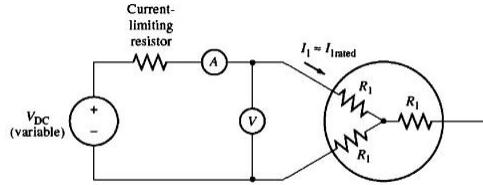


Figure 2.6: Diagram of an induction motor under DC test

The procedures followed to properly do a DC test on an induction motor are.[15, 1]

1. Connecting the induction motor with the DC power supply and the measurement devices.
2. Slowly increasing the power supply input voltage in steps.
3. Recording and noting down the voltage and current readings.

The two ends of the stator windings are linked to the DC input, the current flows through two windings, resulting in a combined resistance of  $2R_1$  in the current’s path.[9, 13, 15]

$$2R_1 = \frac{V_{dc}}{I_{dc}} \quad (2.12)$$

$$R_1 = \frac{V_{dc}}{2I_{dc}} \quad (2.13)$$

By determining the value of  $R_1$ , it is possible to quantify the stator losses in the stator and calculate the  $P_{rotor}$  losses by subtracting the stator losses from the input power  $P_{in}$ .[9, 13, 15]

## 2.3 Measurement methods and signal conditioning

To ensure an accurate characterization of an induction motor, it is essential to utilize robust measurement methods for voltage, current, speed, and torque within the test bench. This section will delve into the sensors, measurement techniques, and circuits that play a vital role in guaranteeing the effective operation of the test bench.

### 2.3.1 Voltage measurement

Voltage measurement, a crucial aspect in the endeavor of characterizing a machine, can be accomplished through a diverse array of methods. This subsection aims to discuss the employed techniques and components that facilitate the attainment of this goal.

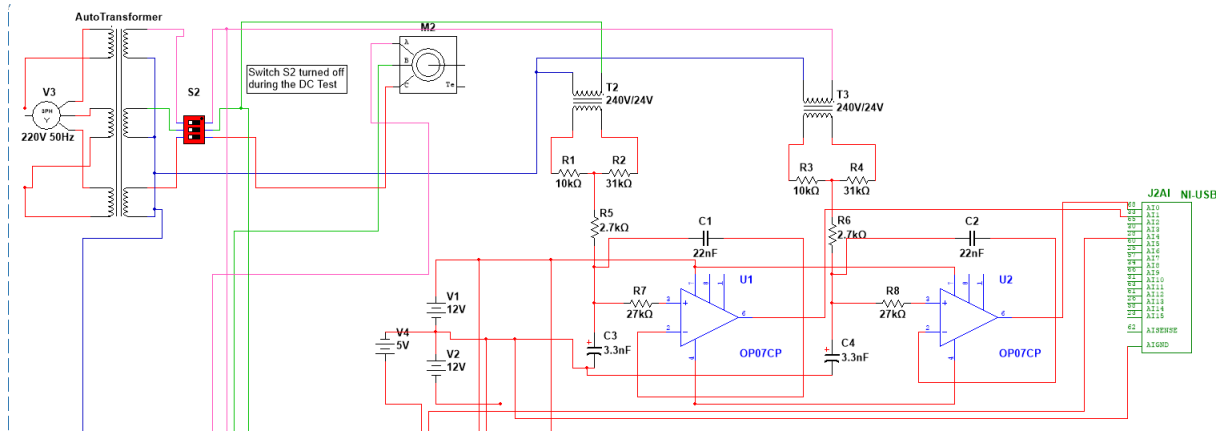


Figure 2.7: Voltage measurement part of the testing circuit

### Voltage Transformers

Transformers are devices comprising of two closely coupled coils. When an AC voltage is applied to the primary coil, it manifests in the secondary coil, resulting in a voltage multiplication that is proportional to the turns ratio of the transformer.[16]

Importantly, it should be noted that power conservation is maintained throughout this process.[16]

To reduce the voltage from the motor to a more manageable level for further processing, 240V/24V transformers were employed. These transformers facilitated the conversion of the motor's high voltage to a lower value before transmitting it to the subsequent voltage divider circuit.

### Voltage Divider

Voltage dividers represent a commonly encountered component in electronic circuits, widely utilized for their simplicity and effectiveness. These circuits efficiently generate a predictable fraction of the input voltage when provided with a specific input.[16]

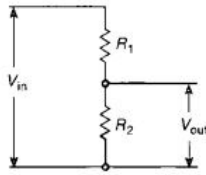


Figure 2.8: Circuit illustrating a voltage divider

The equation illustrating the relationship between the input and output voltages is presented below.[16]

$$\frac{V_{out}}{V_{in}} = \frac{R_2}{R_1 + R_2} \quad (2.14)$$

In order to achieve a safe voltage level of 5.86V for filtering and subsequent transmission to the data acquisition device, the voltage divider circuit was implemented. This circuit effectively reduced the initial 24V from the transformers. The specific configuration involved the use of two resistors, one with a value of 31KΩ and the other with a value of 10KΩ. The output voltage was obtained from the connection point of the 10KΩ resistor. Further details about the data acquisition device will be discussed in the upcoming sections.

### Voltage Measurement Conditioning Circuit

All sensor output signals inherently contain noise, making filtering circuits necessary for accurate measurements. In this specific measurement, a filter circuit is required to suppress frequencies above 24 kHz. This value represents half the sampling frequency of the data acquisition device and was selected to prevent a phenomenon known as aliasing.[18]

The sampling theorem, also known as Shannon's theorem, explains this phenomenon, stating that any frequency exceeding half the sampling frequency (or the "Nyquist rate") will correspond to a frequency between zero and one-half the sampling frequency. This theorem's equation is shown below.[18]

$$f_s > 2f_{max} \quad (2.15)$$

where:

$f_s$  is the sampling frequency (sampling rate) in Hz, indicating how many samples are taken per second.

$f_{max}$  is the maximum frequency component in the signal being sampled in Hz.

If there is already a sinusoidal signal present in this lower frequency range, the aliased signal will combine with it, resulting in a loss of information in both the original sinusoidal signal and the aliased signal. This ultimately leads to a distorted signal when the output signal of the filter is examined using

an oscilloscope.[18]

To effectively attenuate high frequencies, one has the option of employing either a passive or an active low-pass filter. In this case, the decision was made to employ an active filter due to its adjustable nature and flexibility, which allow for enhanced control over the signal.

Additionally, active filters possess a high output impedance, a crucial factor for impedance matching when connected to high input impedance components, thereby preventing signal degradation. To achieve the aforementioned objectives, a 2<sup>nd</sup> order Sallen-key low-pass filter with a cutoff frequency of 3.78 kHz was employed.

The filter was constructed using two resistors, namely  $R_1$  with a value of  $2.7k\Omega$  and  $R_2$  with a value of  $27k\Omega$ , in conjunction with two capacitors, namely  $C_1$  with a capacitance of 22 nF and  $C_2$  with a capacitance of 3.3 nF. The operational amplifier employed for this purpose was an OP07CP which is supplied using +12V DC and -12V DC voltages.

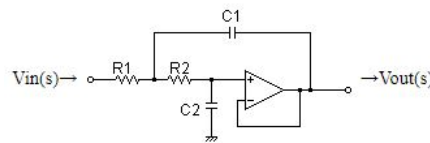


Figure 2.9: 2<sup>nd</sup> Order Sallen-Key Low Pass Filter

## 25V Voltage Sensor Module

The voltage sensing module is essentially a compact board that incorporates a voltage divider. It comprises two resistors, namely  $30k\Omega$  and  $7.5k\Omega$ , and extracts its output voltage from the connection point of the  $7.5k\Omega$  resistor.[17]

The module served the purpose of measuring the DC voltage supplied to the motor during the DC test. It features two inputs, GND and Vcc, which need to be connected to the voltage source under measurement. Additionally, it provides two + and - outputs, as well as a third "S" output, which should be connected to the analog input of the data acquisition device. It is supplied with a 5V DC voltage.[17]

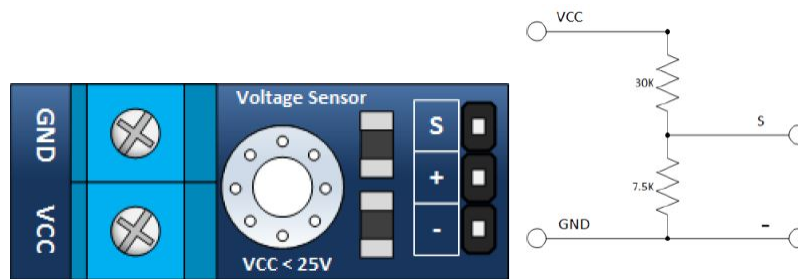


Figure 2.10: Voltage Sensor Module along with its corresponding circuit



## 2.3.2 Current Measurement

Conventional ammeters pose significant risks to testing equipment when used in applications involving high current flow through a machine. This subsection will explore the approaches utilized for measuring high voltage and delve into the utilization of specific physical phenomena, such as the Hall effect, to measure current.

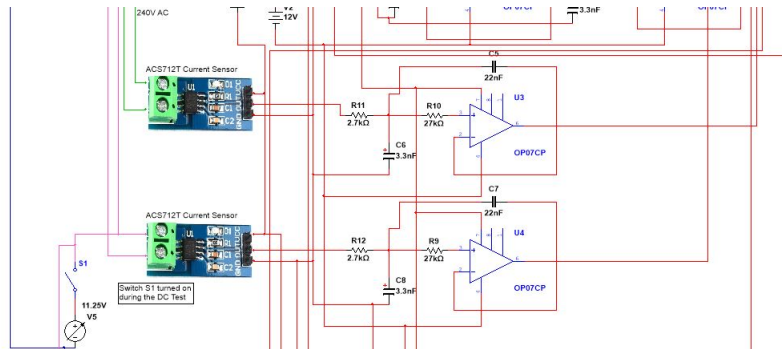


Figure 2.11: Current measurement part of the testing circuit

### ACS712T Current Sensor

The Allegro ACS712 is a reliable and compact solution designed for sensing both AC and DC currents. It finds utility in applications that require isolation of a low-voltage circuit from a high-current source. Typical applications include load detection and management, switched-mode power supplies, and over-current fault protection.[19]

The device comprises a hall sensor circuit with a copper conduction path located near the surface of the die, ensuring accuracy by closely coupling the magnetic circuit with the hall transducer. As current flows through the copper conduction path, a magnetic field is generated, which is then converted into a proportional voltage—this phenomenon is known as the Hall effect.[19]

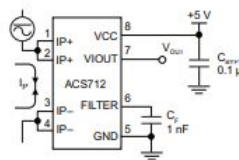


Figure 2.12: Typical application of the ACS712T sensor

The output voltage is generated by a low-offset, chopper-stabilized BiCMOS Hall IC programmed for enhanced accuracy. The output exhibits a positive slope when the current through the primary copper conduction path increases. The sensor, specifically the ACS712ELCTR-20A-T model used here, can accurately sense currents up to 20A.[19]

It operates on a 5V DC power supply. The sensor undergoes meticulous calibration at the factory, allowing it to be used directly with the aid of the Output voltage vs. Sensed current charts provided by the manufacturer.[19]

The robust design of the sensor enables it to withstand five times the rated current without damage, thanks to the thickness of the copper conductors.[19]

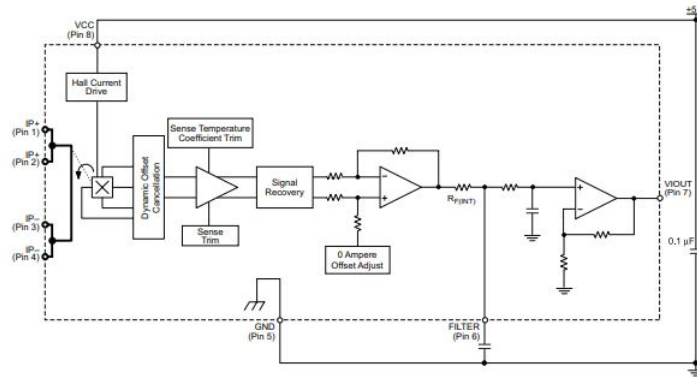


Figure 2.13: Functional Block Diagram of the ACS712T sensor

### Current Measurement Conditioning Circuit

While the voltage output from the current sensor exhibits impressive stability and is free from noise, a 2<sup>nd</sup> order Sallen-Key low pass filter, similar to the one utilized in the aforementioned voltage sensing circuit, was implemented.

The filter employed the same resistor and capacitor values, as well as the same OP07CP operational amplifier.

### 2.3.3 Speed Measurement

Various sensors can be employed for measuring the speed of a motor. These include optical encoders, Hall effect sensors, tachometers, inductive proximity sensors, and magnetic sensors.

This section will elucidate the different types of sensors utilized for speed measurement, their operational principles, and the rationale behind selecting a particular sensor over others.

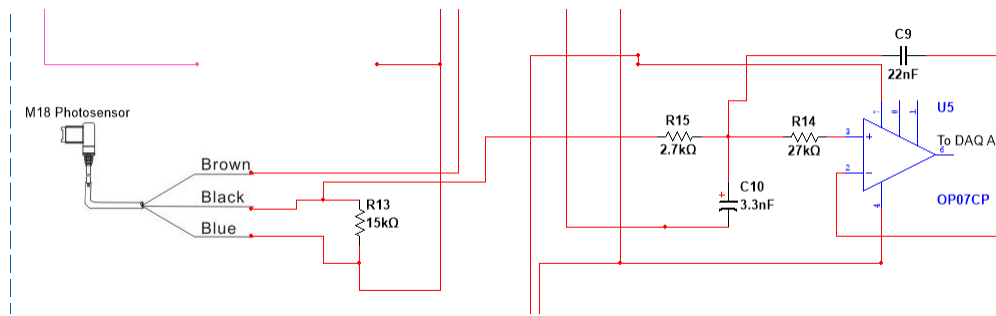


Figure 2.14: Speed measurement part of the testing circuit

### M18 Retro-Reflective Sensor

The decision to utilize a retro-reflective sensor was based on several factors. These include its significantly extended range in comparison to other photoelectric sensors, reduced risk due to its non-contact nature with the motor as opposed to physical sensors, and notably, its capability to accurately measure exceedingly high speeds.[20, 21]

The M18 retro-reflective sensor finds widespread use in various industrial applications, where it serves the purpose of object detection, distance monitoring, and process control. Its operation relies on the principle of light reflection, employing a strategically positioned reflector that faces the sensor. Housed within a compact M18-sized casing, the sensor comprises an emitter and a receiver.[20, 21]



Figure 2.15: Picture of the M18 Retro-Reflective Sensor

The emitter emits a beam of light, typically infrared, directed towards the reflector. The reflector then reflects the emitted light back to the receiver. Upon detection of the light, the receiver registers an impulse with an amplitude corresponding to the supply voltage. For instance, when supplied with 10V DC, the registered impulse will also be 10V DC. Conversely, when no light is reflected, a value of 0V is registered.[20, 21]

During motor operation, the sensor outputs a train of impulses. The sensor features two inputs: one connected to the supply voltage ranging from 10V DC to 30V DC, and the other connected to the common. Additionally, it requires a load connected between the output and the common to ensure proper functioning. A 15KΩ resistor was utilized as the load in this particular setup.[20, 21]

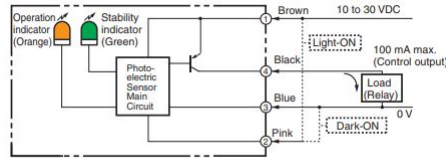


Figure 2.16: Internal Diagram of the M18 Sensor

### Speed Measurement Conditioning Circuit

In order to achieve precise speed measurement, the utilization of a filter is crucial. This is due to the inherent noise generated by the photoelectric sensor, as its receiver is highly sensitive and can capture unintended reflections, such as those from surrounding walls, resulting in a noisy signal.

To address this, the same 2nd order Sallen-Key low pass filter was employed once again to effectively filter the output signal. The purpose was to isolate and capture only the relevant reflections corresponding to the motor’s revolutions. The identical resistor and capacitor values, along with the OP07CP operational amplifier, were utilized in this configuration.

### 2.3.4 Torque Measurement

Torque plays a vital role in characterizing motors since it is a crucial parameter for evaluating performance, analyzing efficiency, optimizing motor design, and diagnosing faults.[22, 23]

Various techniques can be employed to measure torque, including direct measurement using a torque sensor positioned between the shaft and the load, electrical measurement derived from the motor’s electrical parameters, motor slip measurement to infer torque, and the dynamometer method which employs a mechanical device.[22, 23]

This section will delve into these torque measurement methods and provide rationale for the chosen components.[22, 23]

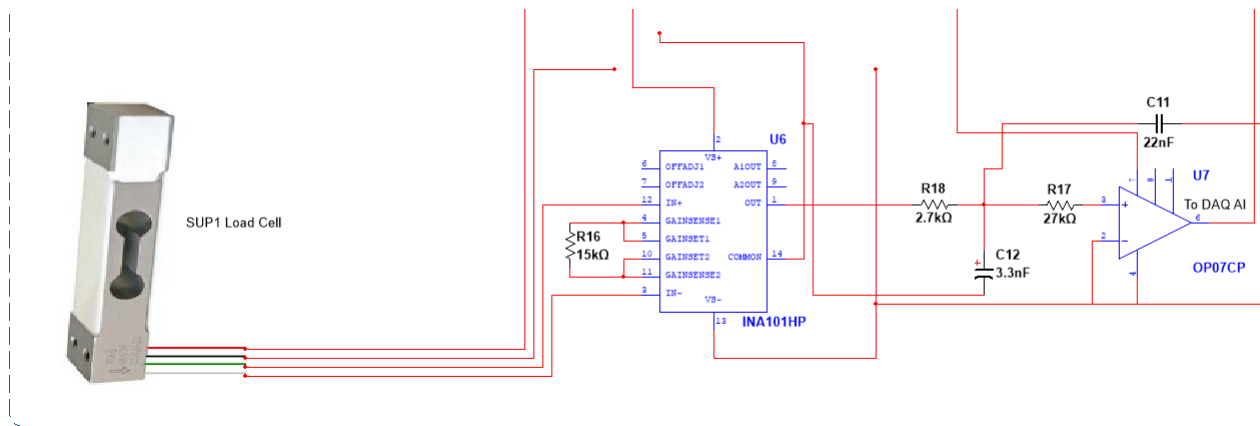


Figure 2.17: Torque measurement part of the testing circuit

## DC Dynamo with a Balance

The DC dynamo, also known as a DC generator, is a device that converts mechanical energy into electrical energy. It consists of two main components: the rotor and the stator. When the rotor rotates, the electromagnets in the stator generate a magnetic field that induces an alternating current (AC) in the coil of wire on the rotor. To obtain direct current (DC), a commutator is used. DC dynamos are commonly used when a steady source of DC power is required.[22, 13, 14]

However, DC dynamos are becoming less popular for converting AC power to DC due to the higher reliability of rectifiers and solid-state devices. In the specific context discussed here, the DC dynamo was employed as a mechanical brake for the motor. This was achieved by connecting the motor's shaft to the dynamo's shaft, and connecting the electrical terminals of the dynamo to two series resistance banks, each with a resistance of 880 ohms, resulting in a combined load of 2090 watts. The DC dynamo was also connected to a 220V DC power supply.[22, 13, 14]

As the motor rotates, it drives the dynamo, which generates electrical energy. This energy is then fed into the connected electrical load. The load acts as a resistance, consuming the electrical energy generated by the dynamo. This resistance provides a braking effect on the motor by opposing its rotational motion.[22, 13, 14]

The dynamo is mounted on a pivoting axis, allowing the motor to transfer its mechanical force to the dynamo when it opposes the rotational motion. The dynamo has two shafts connected on its sides, each with a weight at the end. When the motor encounters resistance from the dynamo, it attempts to rotate its entire body, causing one of the shafts to press its associated weight onto a load cell. The load cell converts the applied force into a voltage, allowing for the identification of torque through calculations discussed in the subsection dedicated to the load cell sensor.[22, 13, 14]

The greater the load applied to the dynamo, the more it slows down the motor and increases its torque by placing additional mechanical stress on the motor, requiring it to work harder. This is how the Speed-Torque graph mentioned in Chapter 2 is created.

## SUP 1 Load Cell

Load cells are force sensing modules that have a meticulously designed metal structure. These modules incorporate small elements known as strain gauges, strategically placed on the structure. The purpose of the load cell is to measure a specific force while disregarding other applied forces. Typically, the load cell's output is in millivolts (mV), ranging from 0V DC to 20 mV DC in the case of the SUP1 model. This indicates that amplification is typically required for the output signal.[24]

Strain-gauge load cells function by converting applied load into electrical signals. The strain gauges are bonded together within a beam or structural member, which undergoes deformation when subjected to weight. Consequently, the strain gauges themselves deform, leading to a change in their electrical resistance that is proportional to the load.[24]

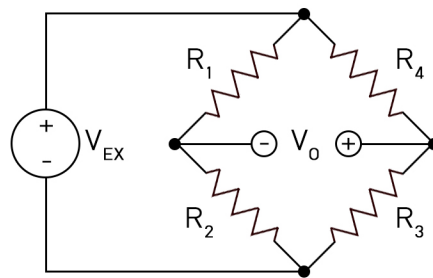


Figure 2.18: Strain Gauges arranged in a Wheatstone Bridge

To compensate for variations in resistance caused by temperature changes, most load cells employ four strain gauges. Some of these gauges operate under compression, while others experience tension, maximizing sensitivity and automatically mitigating the effects of temperature.[24]

The strain gauges are arranged in a Wheatstone bridge configuration. To obtain accurate readings, the load cell's output needs to be calibrated by applying various loads and simultaneously recording the resulting output. As shown in the table below.

Applied Weight (Kg)	Recorded Amplified Output (V)
0	4.88
0.5	4.96
1	5.04
1.5	5.12
2.5	5.28

It should be mentioned that the original output voltage from the load cell was amplified 34.33 times.

The SUP1 load cell can be supplied with an input voltage ranging from 0.1V DC to 15V DC.[24]

It has two input wires: the red wire connected to the +12V DC and the black wire connected to the -12V DC. Additionally, there are two green and white wires between which the output signal should be measured and then sent to the amplifier circuit.[24]

Based on the data obtained during the on-site calibration, the subsequent formula was established.

$$Torque = 18.3937V_{out} - 18.3937V_{out-rest} \quad (2.16)$$

where.

$V_{out}$  is the amplified output voltage coming from the load cell while the motor is running.

$V_{out-rest}$  is the amplified voltage coming from the load cell while the motor is turned off.

Considering the load cell's high sensitivity and the vibrations emitted by the operating motor, it was decided to make the offset  $V_{out-rest}$  "dynamic," allowing the user to input it before starting the testing process. This approach aims to ensure the best possible results.

The torque formula was derived by applying fundamental principles of physics along with the utilization of these two equations.

$$F = m \times 9.81 \quad (2.17)$$

Where.

F is the force being applied on the load cell.

m is the mass the balance's attached weight is producing. Which was determined using the calibration chart of the load cell.

$$T = F \times r \quad (2.18)$$

Where.

r is the distance between the point of force application and the axis of rotation. Which was 0.3m.

### **Torque Measurement Voltage Conditioning**

Although the load cell's output exhibits relatively stable characteristics when compared to the output of the speed sensor, it was decided to employ the identical 2nd order Sallen-Key low-pass filter used in the

previous filter circuits. This involved utilizing the same resistor and capacitor values in conjunction with the OP07CP operational amplifier.[25]

When dealing with the load cell, it is crucial to incorporate an amplification circuit because of the extremely low output it generates. The decision was made to utilize the INA101HP, a robust and dependable High Accuracy Instrumentation Amplifier manufactured by Texas Instruments (TI).[25]

The INA101 is an instrumentation amplifier known for its high accuracy, specifically designed for amplifying low-level signals and serving general-purpose data acquisition purposes. It integrates three precise operational amplifiers and laser-trimmed metal film resistors onto a single monolithic integrated circuit.[25]

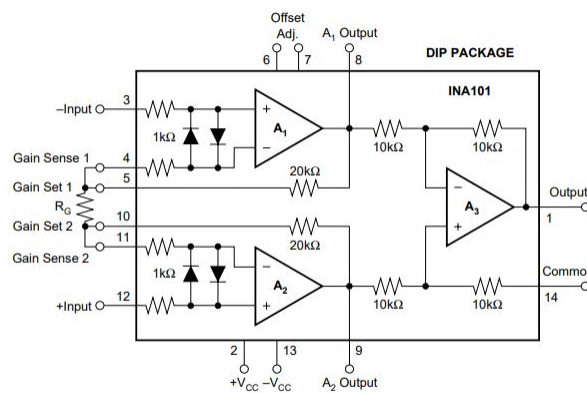


Figure 2.19: Internal Diagram and Basic Connections of the INA101

The amplification gain of the INA101 can be established by connecting a single external resistor, denoted as  $R_G$ , which determines the gain according to the provided formula.[25]

$$G = 1 + \frac{40K\Omega}{R_G} \quad (2.19)$$

The value of  $40K\Omega$  originates from the two internal feedback resistors, which are meticulously trimmed via laser to ensure precise absolute values.

However, when aiming for higher gains and using lower resistance values for  $R_G$ , the presence of wiring resistance, especially in the case of sockets, can contribute to additional gain errors, particularly for gains around or exceeding 100. To exemplify, a gain of 34.33 was successfully achieved using a  $1.2K\Omega$  resistor.[25]

The typical operating voltage employed for the INA101 was  $\pm 12V$  DC, aligning with its specified supply voltage range.



## 2.4 LabVIEW and DAQ

### 2.4.1 LabVIEW

LabVIEW (Laboratory Virtual Instrument Engineering Workbench) is a widely used graphical programming environment in research and industry. It serves as a powerful and versatile analysis and instrumentation software for measurement and automation. LabVIEW is based on G programming, a graphical block diagram language that compiles into machine code, eliminating the need for intricate syntax. This software-based platform offers exceptional flexibility, surpassing standard laboratory equipment.[26]

LabVIEW programs are referred to as virtual instruments (VIs) due to their resemblance to physical instruments. It encompasses a diverse collection of VIs and functions for data acquisition, analysis, display, and storage. Additionally, it provides tools to aid in code troubleshooting. LabVIEW can acquire data from various devices, including PXI instruments, Serial, DAQ, and PLC. Its functionalities encompass differential equations, curve fitting, linear algebra, and calculus, facilitating the analysis and processing of acquired data. The software also provides a range of data representation tools such as gauges, meters, graphs, and charts.[26]

The LabVIEW family includes NI LabVIEW graphical programming for measurement and automation, LabVIEW real-time module, LabVIEW FPGA module, LabVIEW PDA module, LabVIEW data logging and supervisory module, as well as several other modules and addons that simplify tasks and minimize the need for extensive and repetitive programming. The details regarding the utilized toolkits, addons, and modules will be discussed shortly.[26]

While a simple physical HMI combined with an Arduino board or PLC could have been chosen, the decision was made to employ a computer with LabVIEW as the "brain" of the testing circuit. This choice was driven primarily by the ease of customizing the interface with minimal alterations to the physical circuit. Moreover, LabVIEW programming provides accessibility, saving time that would otherwise be spent on learning syntax and allowing more focus on refining the design. Cost is also a factor, as a computer equipped with LabVIEW is significantly more affordable than a decent PLC, and a computer offers greater versatility as it is not limited to specialized functions.[26]

Although LabVIEW code is a high-level language, it exhibits comparable compiling speed to the C language. When used with NI hardware, such as the NI USB series data acquisition devices, the need for creating driver circuits or programs is eliminated, enabling full concentration on the software aspect. This combination of LabVIEW and NI DAQ presents an intriguing, cost-effective, and versatile choice, particularly for small-scale applications where cost considerations play a significant role.[26]

A brief explanation will be provided regarding the three steps involved in creating a LabVIEW application.

## Front Panel Window

The front panel serves as the interactive user interface of the VI, resembling the physical front panel of an instrument. It enables the operation of the instrumentation program, control of specific hardware, analysis of acquired data, and display of results. Knobs, push buttons, and other controls are positioned on the front panel.[26]

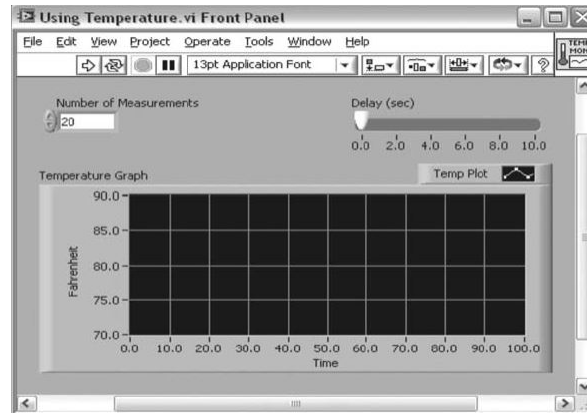


Figure 2.20: LabVIEW virtual instrument front panel.

## Block Diagram Window

The block diagrams are an integral part of the program, accompanying the front panel. The front panel objects are represented as terminals on the block diagram, and these components are connected together through wiring. Once the front panel is constructed, codes are incorporated using graphical representations of functions on the block diagram to control the front panel objects.[26]

The block diagram comprises nodes, terminals, and wires, forming the graphical source code. It includes lower-level VIs, built-in functions, constants, and program execution control structures. Wires are drawn to establish connections between corresponding objects, indicating the flow of data between them. The front panel objects have corresponding terminals on the block diagram, facilitating the seamless passage of data between the user and the program.[26]

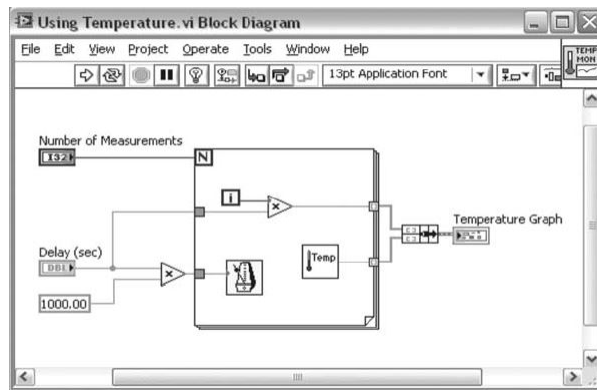


Figure 2.21: LabVIEW virtual instrument block diagram.

### Icon/Connector Pane

To utilize a VI as a subVI, it is necessary for it to possess both an icon and a connector pane. Each VI exhibits an icon located in the upper-right corner of the front panel and block diagram windows, serving as a graphical representation of the VI. The icon can consist of text and images. When employing a VI as a subVI, a connector pane needs to be constructed. This connector pane comprises terminals that correspond to the controls and indicators present in the VI.[26]

During the development of the program, a variety of LabVIEW modules, addons, and functions were employed. The following overview will give a brief summary of these components.

### XY Graph Plotting

The XY graph accepts three types of data for single-plot XY graphs. Firstly, it accepts a cluster consisting of an x array and a y array. Secondly, it accepts an array of points, where each point is represented by a cluster containing an x value and a y value. Lastly, it accepts an array of complex data, where the real part is plotted on the x-axis and the imaginary part is plotted on the y-axis.[26]

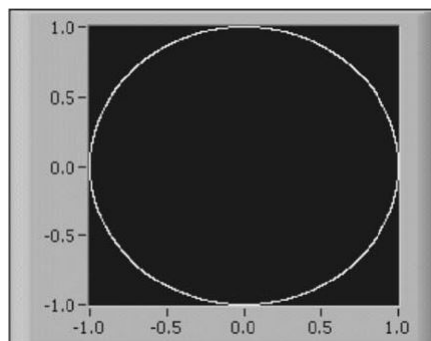


Figure 2.22: An XY graph.

## Waveform Graph plotting

The waveform graph offers several options for data types when creating single-plot waveform graphs. Firstly, it accepts a single array of values, interpreting the data as points on the graph with the x index starting at 0 and incrementing by one. Secondly, it accepts a cluster consisting of an initial x value, a delta x, and an array of y data. This allows for more precise control over the x-axis values.[26]

Furthermore, the waveform graph supports the waveform data type, which contains the waveform's data, start time, and delta t (time increment) information. This data type is specifically designed for waveform representation. Additionally, the graph accommodates the dynamic data type, primarily used with Express VIs (Virtual Instruments). The dynamic data type includes not only the signal data but also attributes providing information about the signal, such as its name, acquisition date, and time. These attributes determine the appearance of the signal on the waveform graph.[26]

In cases where the dynamic data type contains a single numeric value, the graph plots that value and automatically formats the plot legend and x-axis time stamp accordingly. Similarly, when the dynamic data type includes a single channel, the graph plots the entire waveform and adjusts the plot legend and x-axis time stamp accordingly.[26]

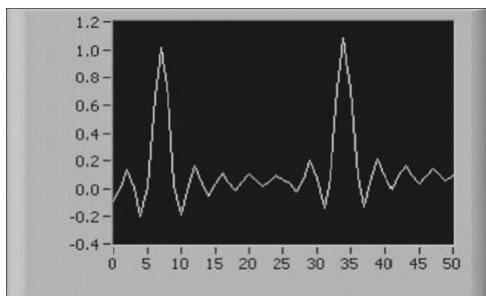


*Figure 2.23: Waveform Graph.*

## Tone Measurement Function

In LabVIEW, the tone measurement function is a powerful tool used for analyzing and measuring audio tones or frequencies within a given signal. It allows users to perform comprehensive analysis of audio signals, aiding in tasks that require accurate frequency identification and measurement.[27, 26]

The tone measurement function in LabVIEW operates by utilizing the fast Fourier transform (FFT) algorithm to decompose the input signal into its frequency components. By applying the FFT, the function provides a spectrum representation of the signal, revealing the presence and strength of various frequencies.[27, 26]

LabVIEW offers a range of built-in functions and tools for tone measurement, enabling users to configure essential parameters such as the sampling rate, windowing technique, and frequency resolution for the FFT analysis. Additionally, LabVIEW provides various options for displaying the results, including

graphical representations such as spectrograms and numerical outputs.[27, 26]

With the tone measurement function in LabVIEW, users can extract valuable information about audio signals. This includes identifying specific frequencies, measuring their amplitudes, and detecting harmonic content. This capability is particularly useful in audio processing, sound engineering, and other applications where precise tone analysis is required.[27, 26]

By utilizing the tone measurement function in LabVIEW, users can gain insights into audio signals, perform detailed frequency analysis, characterize frequency responses, and facilitate tasks such as tone identification. The flexibility and functionality of LabVIEW's tone measurement tools make it an essential resource for professionals working with audio signals and frequencies.[27, 26]

### **Waveform Scale and Offset**

The waveform scale and offset function in LabVIEW is a versatile tool that allows users to manipulate and adjust the scaling and offset of waveform data. It is particularly useful in tasks involving waveform visualization, signal processing, and data analysis. With the waveform scale functionality, users can modify the range or magnitude of the waveform values along both the x-axis (time) and y-axis (amplitude). Scaling enables users to amplify or attenuate the amplitude of the waveform data, effectively zooming in or out to focus on specific details or visualize the entire waveform more clearly.[27, 26]

The waveform offset feature complements the scaling functionality by enabling users to vertically shift the entire waveform data. This capability proves particularly useful when aligning waveforms with reference lines, other waveforms, or specific measurement thresholds. By applying vertical offsets, users can align waveforms to a desired position, making it easier to compare and analyze signal characteristics accurately. These capabilities enhance the flexibility and adaptability of waveform visualization in LabVIEW, empowering users to tailor the representation of waveform data according to their specific analysis requirements.[27, 26]

### **NI Device Monitor**

The NI Device Monitor is a software tool provided by National Instruments (NI) that allows users to monitor and manage NI hardware devices connected to a computer. It provides a centralized interface to view and control various aspects of the connected devices, including their status, configuration, and performance.[27, 26]

The NI Device Monitor offers real-time monitoring capabilities, displaying critical information such as device health, firmware version, connection status, and any potential issues or errors. It provides a comprehensive overview of the connected NI devices, making it convenient for users to keep track of their hardware assets.[27, 26]

In addition to monitoring, the NI Device Monitor enables users to configure and manage device settings. It allows users to adjust parameters such as sample rates, trigger settings, channel configurations,

and input/output modes. This flexibility empowers users to customize and optimize device settings to suit their specific application requirements.[27, 26]

The NI Device Monitor also facilitates firmware updates for compatible NI devices. It provides a streamlined process to check for firmware updates and perform the necessary upgrades, ensuring that devices are running the latest firmware versions with enhanced features and bug fixes.[27, 26]

Furthermore, the NI Device Monitor may include diagnostic tools and troubleshooting capabilities. It can help users identify and troubleshoot device-related issues by providing detailed error information, status logs, and system diagnostics. This aids in the efficient resolution of problems and improves the overall reliability of the NI hardware devices.[27, 26]

## **NI-DAQmx**

NI-DAQmx is a software framework developed by National Instruments (NI) for data acquisition and control applications. It provides a unified programming interface and driver software that allows users to interact with NI data acquisition (DAQ) devices, such as analog input/output modules, digital I/O modules, and counter/timer modules.[27, 26]

NI-DAQmx simplifies the process of acquiring, generating, and analyzing data from various sensors and signals. It offers a comprehensive set of functions and configuration options to handle tasks such as signal conditioning, data acquisition, synchronization, and control of DAQ devices.[27, 26]

With NI-DAQmx, users can configure the sampling rate, voltage range, and other acquisition parameters to suit their specific application requirements. The framework supports a wide range of sensor types and signal formats, including voltage, current, temperature, strain, frequency, and digital signals.[27, 26]

One of the key features of NI-DAQmx is its intuitive programming interface. It provides a high-level API that allows users to easily develop data acquisition and control applications using popular programming languages such as LabVIEW, C, C++, and C#. The API offers a rich set of functions for device configuration, data acquisition, triggering, and synchronization.[27, 26]

NI-DAQmx also includes advanced features like hardware-timed signal generation, onboard signal processing, and synchronization capabilities for multi-device setups. It supports real-time data streaming, precise timing control, and synchronization between multiple DAQ devices, enabling the development of complex measurement and control systems.[27, 26]

## **LabVIEW Electrical Power Toolkit**

The LabVIEW Electrical Power Toolkit provides a comprehensive set of tools and functions for calculating power in electrical systems. It utilizes various mathematical algorithms and formulas to accurately determine active, reactive, and apparent power.[27]

To calculate active power, the toolkit uses measurements of voltage and current. It applies mathematical operations such as multiplication and integration to obtain the instantaneous power at each point in time. By integrating the product of voltage and current over time, LabVIEW can accurately calculate the active power consumed or produced by a load or device. This information is crucial for understanding energy consumption, optimizing power usage, and analyzing power flows in a system.[27]

For calculating reactive power, the Electrical Power Toolkit employs trigonometric functions and complex number operations. It considers the phase shift between voltage and current, which occurs due to inductive or capacitive loads. By quantifying the reactive component of power using measurements of voltage and current, LabVIEW can determine the reactive power in the system. This information is essential for power factor analysis, load balancing, and optimizing power factor correction devices.[27]

The toolkit also enables the calculation of apparent power, which is the vector sum of active and reactive power. By combining the calculated active and reactive power values, LabVIEW accurately determines the total power being supplied or consumed by an electrical system. This information is useful for sizing electrical components, evaluating system capacity, and ensuring efficient power distribution.[27]

LabVIEW’s Electrical Power Toolkit incorporates advanced algorithms and functions that handle various aspects of power calculations, including voltage and current waveform analysis, complex number manipulation, and integration techniques. These algorithms are designed to handle the complexities of AC power systems, enabling accurate and reliable power calculations.[27]

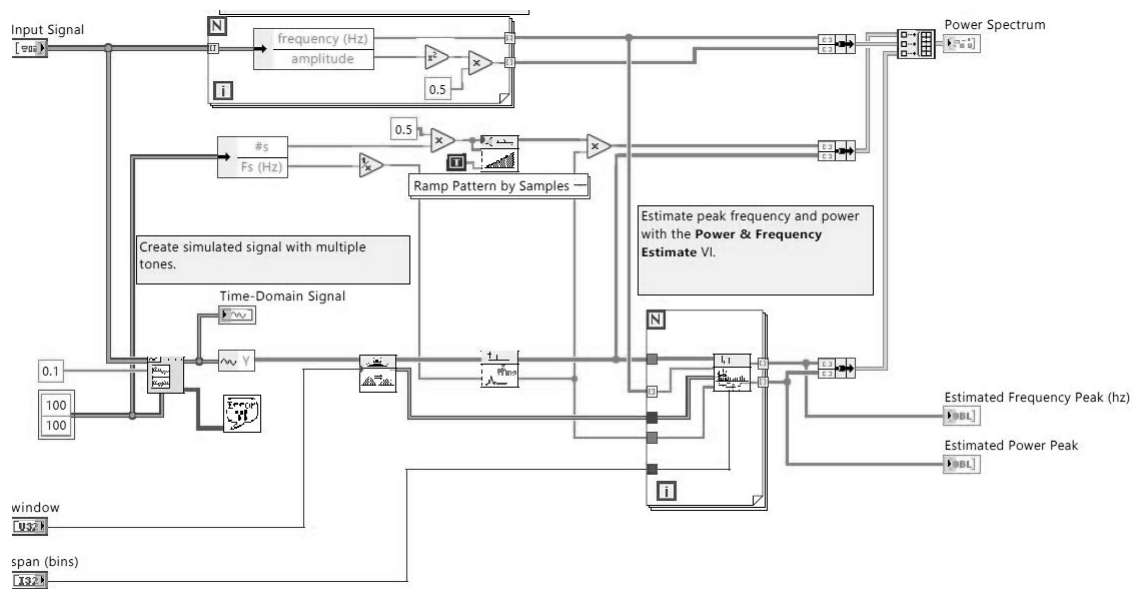


Figure 2.24: Example of a Power and Frequency Estimator using the LabVIEW Electrical Power Toolkit

### Labview Digital Filter Design Toolkit

The LabVIEW Digital Filter Design Toolkit is a specialized add-on module for LabVIEW, offered by National Instruments (NI). It provides engineers and researchers with a comprehensive set of tools and

functions for designing, analyzing, and implementing digital filters.[27]

With the Digital Filter Design Toolkit, users can design a wide range of digital filters to process and manipulate signals. This includes finite impulse response (FIR) filters, infinite impulse response (IIR) filters, and adaptive filters. The toolkit offers various design methods and algorithms, such as windowing, frequency sampling, and least squares, to meet specific filtering requirements.[27]

The toolkit provides an intuitive graphical user interface (GUI) that simplifies the filter design process. Users can interactively specify filter parameters, such as filter type, cutoff frequency, filter order, and filter response characteristics. The toolkit then generates the corresponding filter coefficients or transfer function, ready for implementation in LabVIEW or other digital signal processing systems.[27]

One of the key features of the Digital Filter Design Toolkit is its ability to analyze and evaluate filter performance. Users can simulate and analyze the frequency response, phase response, and impulse response of the designed filters. This allows for fine-tuning and optimization of the filter design to achieve the desired signal processing goals.[27]

Furthermore, the Digital Filter Design Toolkit supports filter implementation and integration within LabVIEW applications. Users can seamlessly integrate the designed filters into their LabVIEW projects, enabling real-time signal processing, data analysis, and control applications. The toolkit provides easy-to-use functions and libraries for filter implementation, allowing users to process signals efficiently and effectively.[27]

The LabVIEW Digital Filter Design Toolkit is suitable for a wide range of applications, including audio processing, communication systems, image processing, biomedical signal analysis, and industrial automation. It empowers users to design and implement custom digital filters tailored to their specific signal processing requirements.[27]

## **2.4.2 Data Acquisition Device**

The data acquisition (DAQ) system utilizes a data acquisition device to transmit a conditioned signal to a computer for software analysis and data logging. Various data acquisition devices can be employed, including those compatible with the PCI bus, PXI bus, IEEE 1394 port, and computer USB, as seen in the test bench scenario.[27]

This section will thoroughly elucidate the operational principle of data acquisition devices while presenting a comprehensive overview of the specific DAQ device employed, its configuration, and its utilization in conjunction with LabVIEW software.

### **NI USB-6009**

The NI USB-6009 is a data acquisition device that provides a range of analog and digital input/output options, making it a versatile tool for data acquisition and control tasks. On the input side, it typically offers multiple analog input channels, allowing users to measure voltage or current signals from external



sources. These input channels are equipped with programmable input ranges, enabling precise measurements across a wide range of signal amplitudes.[27]

Additionally, the device includes analog output channels, which allow users to generate voltage or current signals to control external devices or systems. The analog outputs can be used for tasks such as generating control signals, simulating sensor outputs, or driving actuator circuits.

It provides 8 single-ended analog input channels and 2 analog output channels. These analog input channels allow for the measurement of voltage or current signals from external sources, while the analog output channels enable the generation of voltage or current signals to control external devices.[27]

In addition to the analog channels, the NI USB-6009 also offers 12 digital I/O lines. These digital lines can be configured as inputs or outputs, providing flexibility for interfacing with digital signals or devices. The digital I/O lines are commonly used for tasks such as reading digital sensors, monitoring switch states, or controlling digital actuators. It has a maximum sampling rate of 48KHz.[27]

Alongside the analog and digital channels, the NI USB-6009 also features a built-in 32-bit counter/timer, which can be used for tasks such as frequency measurement, event counting, or generating precise timing signals.

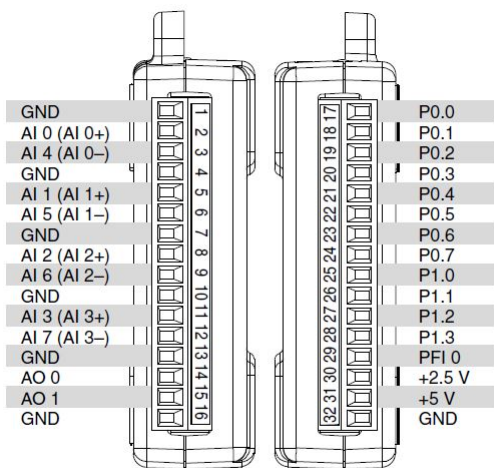


Figure 2.25: Pinout of the NI USB-6009

## DAQ Software Architecture

National Instruments data acquisition boards utilize driver engines to facilitate communication between the board and the application software. Two distinct driver engines are available: NI-DAQmx and Traditional NI-DAQ. LabVIEW can be utilized to establish communication with these driver engines. The DAQ Assistant, an Express VI within LabVIEW, enables communication with the data acquisition board. Additionally, Measurement & Automation Explorer (MAX) serves as a valuable tool for configuring and testing the data acquisition boards.[26]

The driver software serves as an intermediary layer that directly interacts with the registers of the DAQ hardware, overseeing its operation and integration with computer resources such as processor interrupts and memory. By abstracting the complex details of hardware programming, the driver software provides users with an accessible interface or standalone application program.[26]

### **Setting up the NI USB-6009**

To set up the NI USB-6009, one shall:[27, 28]

- Obtain the NI-DAQmx Driver: By visiting the National Instruments website and downloading the latest version of the NI-DAQmx driver software. While making sure to choose the version compatible with the used operating system. Lastly, saving the installation file to the computer.
- Install the NI-DAQmx Driver: By locating the downloaded installation file and running it. Following the on-screen instructions to install the NI-DAQmx driver software. During the installation process, one may be prompted to restart the computer. Once the installation is complete, the necessary software components will be installed for communication with the USB-6009 device.
- Connect the USB-6009: By taking the USB connector of the USB-6009 device and plugging it into an available USB port on the computer. Lastly, ensuring that the connection is secure.
- Configure the Device in Measurement & Automation Explorer (MAX): By launching the NI Measurement & Automation Explorer (MAX) software. One can find it in the list of installed programs. Once MAX opens, it will detect the connected USB-6009 device automatically.
- Device Detection: In the MAX toolbar, clicking on the "Refresh" button to ensure that the USB-6009 is detected. It will appear under the "Devices and Interfaces" section.
- Device Configuration: By right-click on the USB-6009 device and selecting "Create New Task." A configuration window will open, where one can specify the desired settings for the data acquisition tasks, such as the sampling rate, input channels, output channels, and triggering options. Adjusting the settings according to your requirements and clicking "Finish" to save the configuration.
- Develop an Application: With the USB-6009 set up and configured, one can start developing an application using LabVIEW or other supported programming languages. Utilizing the appropriate APIs and libraries provided by National Instruments to communicate with the USB-6009 and performing data acquisition, analysis, and control tasks.

## DAQ Assistant

The DAQ Assistant is a graphical interface that allows users to interactively create, edit, and run NIDAQmx virtual channels and tasks. A virtual channel in NI-DAQmx comprises a physical channel on a DAQ device and the associated configuration information, such as input range and custom scaling. On the other hand, a task in NI-DAQmx is a collection of virtual channels, timing and triggering details, and other properties related to data acquisition or generation.[27]

The DAQ Assistant serves as a user-friendly guide for configuring, testing, and acquiring measurement data. It simplifies the development of complex operations by providing a code generation feature based on the user's configuration.

When the DAQ Assistant Express VI is placed on the block diagram, it launches to create a new task. To modify an existing task, one can double-click the DAQ Assistant Express VI. If continuous measurement or generation is required, it is recommended to enclose the DAQ Assistant Express VI within a While Loop. Wiring the stop condition into the stop input of the DAQ Assistant Express VI is a good practice when using it within a While Loop.[27]

It is important to note that the DAQ Assistant Express VI creates a task that is only accessible within the Express VI. To make the task globally accessible from any application, one must convert the Express VI to an NI-DAQmx task and save it in Measurement & Automation Explorer (MAX). Starting from LabVIEW 8.0, there is the option to generate NI-DAQmx API code from the DAQ Assistant Express VI.[27]

This feature allows the user to generate both configuration and example code for the task by right-clicking the DAQ Assistant Express VI and selecting "Generate NI-DAQmx Code" from the shortcut menu. However, for continuous single-point input or output, it is worth noting that the DAQ Assistant Express VI may not provide optimal performance. In NI-DAQmx, virtual channels play an integral role in every measurement process.[27]

## Creating a Task

To illustrate, consider creating a straightforward input measurement. Specify the analog task for the measurement. For different measurement and signal generation types. One should.[26]

On the initial screen, choose "Analog Input" as the measurement type.

Next, select voltage.

On the following screen, the user will be prompted to select the physical channel(s) for which the task is being created. The tree control will display all supported DAQ devices, and one can expand each device to reveal a list of the available physical channels that can be utilized for task creation.[26]

Click on the "Finish" button, which will advance you to the configuration stage.



Figure 2.26: Analog input measurement.

## Configuring a Task

Once the task is created, one can proceed to configure channel-specific settings, including scaling, input limits, and terminal configuration. Additionally, there is the option to configure task-specific settings such as timing and triggering. For this particular task, scaling and triggering are not required. Instead, one can focus on configuring settings such as range (which determines the gain), terminal configuration, custom scaling, and launching the test panel. To configure the voltage measurement task, one shall.[26]

Specify the input limits for the task. If one is unsure of the theoretical limits for the signal you are measuring, he can utilize the default values of 5 for the maximum limit and -5 for the minimum limit.[26]

Select the terminal configuration that was used for the signal.[26]

On the Task Timing tab, choose the "Acquire N Samples" option. Enter a value of 100 for "Samples To Read" and enter 1000.00 for "Rate" in Hz, as demonstrated below.[26]

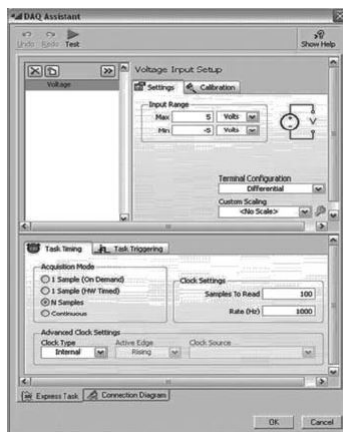


Figure 2.27: Configuration of the Task

## 2.5 Conclusion

In conclusion, Chapter 2 focused on the methods and measurement system employed for testing induction motors. The chapter commenced with an introduction to provide an overview of the objectives and purpose of the chapter. Classical tests commonly used for assessing the performance of induction motors were discussed, including the locked rotor test, no-load test, and DC test. Each test was explained in terms of its setup, measurements, and the information it provides about motor characteristics.

The chapter further delved into measurement methods and signal conditioning techniques utilized in the testing process. Voltage measurement methods, including direct measurement and potential transformer-based measurement, were explored. Current measurement techniques, such as shunt resistor measurement and current transformer-based measurement, were also discussed. Additionally, speed measurement methods involving tachometers, encoders, and proximity sensors were outlined. The torque measurement techniques used to quantify the mechanical output of the motor were elucidated as well.

A significant portion of the chapter focused on the utilization of LabVIEW and a Data Acquisition Device (DAQ) in the testing process. LabVIEW, a powerful programming environment, was highlighted for its ability to facilitate data acquisition, control, and analysis. The integration of LabVIEW with a DAQ system allowed for the collection and processing of sensor signals to obtain accurate measurements of motor parameters.

By employing the methodologies and measurement system described in this chapter, researchers and engineers can effectively evaluate and characterize the performance of induction motors. The information garnered from these tests and measurements serves as a vital foundation for the subsequent chapters, where the developed platform and testing procedures will be presented to achieve the objectives of this thesis.

# Chapter 3

## Developed Platform Description and Testing

### 3.1 Introduction

This chapter presents the results and discussions of the parameter characterization of the three-phase AC motor using LabVIEW. The objective of this study was to investigate and understand the motor's performance characteristics by conducting three different tests: the no-load test, blocked rotor test, and DC test. LabVIEW was utilized as the software platform to collect data and analyze the motor's behavior. To enhance the usability and convenience of the LabVIEW interface, separate tabs were created for each test, allowing for organized and focused analysis.

The Home tab served as the central location for monitoring and analyzing the motor's performance parameters, including voltage, current, and high current alerts. The No Load Test, Blocked Rotor Test and DC Test tabs tab visualized current, voltage, power, and derived parameters, enabling the calculation losses. The Speed-Torque tab visualized instantaneous RPM and torque and included a graph illustrating the torque-speed relationship. This tab allowed for the assessment of the motor's performance curve and determination of its maximum torque and speed capabilities. The final calculation tab aggregated data and derived motor parameters for comprehensive performance evaluation, including efficiency, power factor, and losses.

It facilitated comparisons with industry standards and aided in motor selection and system design. Due to the limited number of analog inputs present in the DAQ 6009, data collection was limited to only two phases of the three-phase AC motor. Despite this limitation, the motor's stable operation allowed for reliable analysis and characterization using the available data. The interface effectively visualized and presented the measurements obtained from the two phases, including voltage, current. Although data from two phases may not provide a complete picture, it was sufficient to gain insights into the motor's performance and behavior under different operating conditions.

The characterization will be carried out semi-automatically by the test bench. The user will be guided by visual illustrations, which show the required wiring. These illustrations will help the user execute the necessary tests and determine the parameters of the induction motor.



Figure 3.1: Nameplate of the used induction motor



Figure 3.2: Nameplate of the used dynamo

## 3.2 Tab Control Interface

### 3.2.1 Home tab

The Home tab within the LabVIEW interface provided a consolidated view of essential measurements for the three-phase AC motor. It served as a central location for observing and analyzing the motor's performance parameters in real-time. The Home tab displayed voltage, current, RPM, torque, and included a high current alert to ensure safety when exceeding the motor's rated current.

This tab will allow researchers to monitor the motor's behavior through realtime voltage and current graphs, providing valuable insights into its electrical performance. While conducting each test, the data visualized in the Home tab undergoes changes to reflect the specific measurements and parameters relevant to that particular test. The Home tab serves as a consolidated view where the real-time data is displayed and updated accordingly.

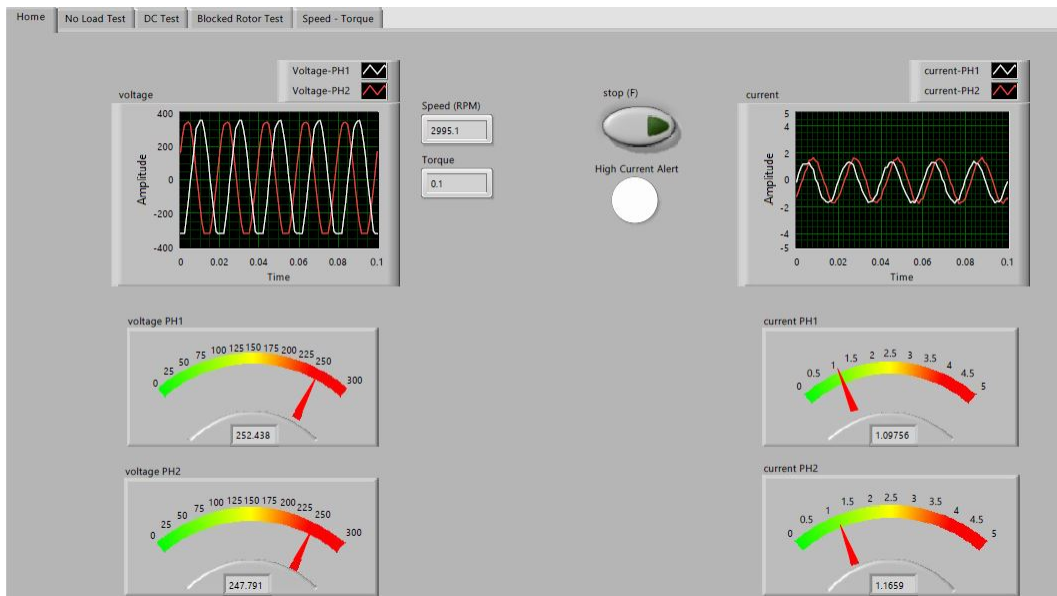


Figure 3.3: Home Tab during the No-Load Test



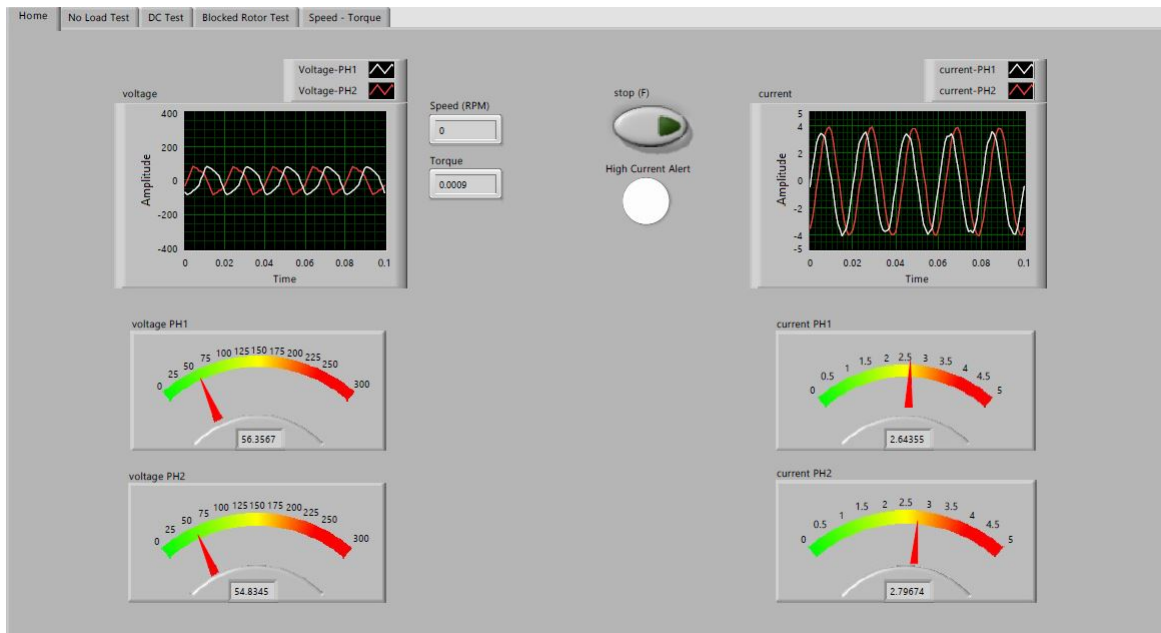


Figure 3.4: Home Tab during the Blocked Rotor Test

### 3.2.2 No Load Test tab

While the Home tab provides a comprehensive view of the motor's performance parameters in real-time, the No Load Test tab is specifically dedicated to visualizing and analyzing the data relevant to the no-load test. The Home tab serves as a broader monitoring tool, whereas the No Load Test tab focuses on specific parameters and measurements related to the no-load condition of the motor.

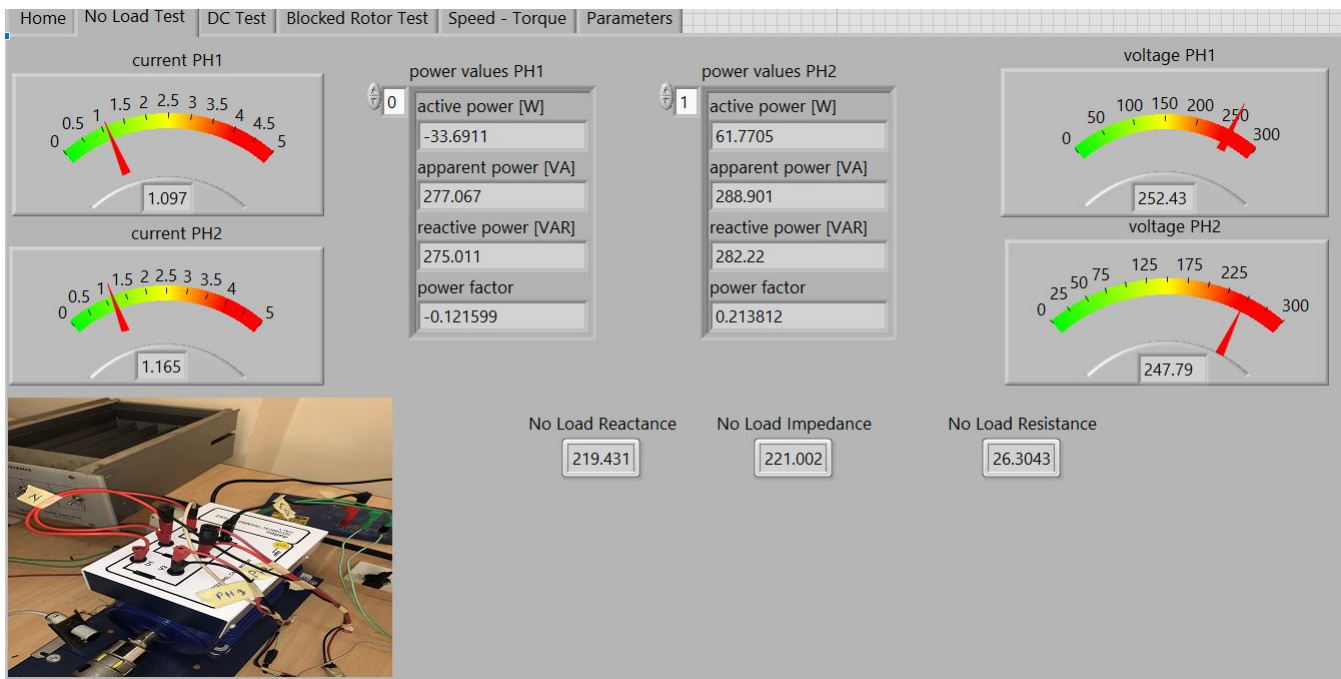


Figure 3.5: No Load Tab during the No Load Test

By utilizing the data visualized in the No Load tab, researchers could gain valuable information regarding the motor's efficiency and losses when operating without any mechanical load. Additionally, this test aided in estimating the motor's power factor, which is a vital parameter in assessing the motor's electrical performance while running on its rated voltage.

The availability of real-time measurements and derived parameters in the No Load tab facilitated accurate analysis and enabled a comprehensive understanding of the motor's electrical behavior during no-load conditions. The derived values of No Load Reactance, No Load Resistance, and No Load Impedance offered valuable insights into the motor's impedance characteristics and further contributed to the overall characterization of the three-phase AC motor.

### 3.2.3 Blocked Rotor Test tab

The Blocked Rotor Test tab in the LabVIEW interface is designed to perform the blocked rotor test on the three-phase AC motor. Unlike the previous test, where the motor operated under normal conditions, the blocked rotor test simulates a scenario where the motor is subjected to a blocked or stalled condition.

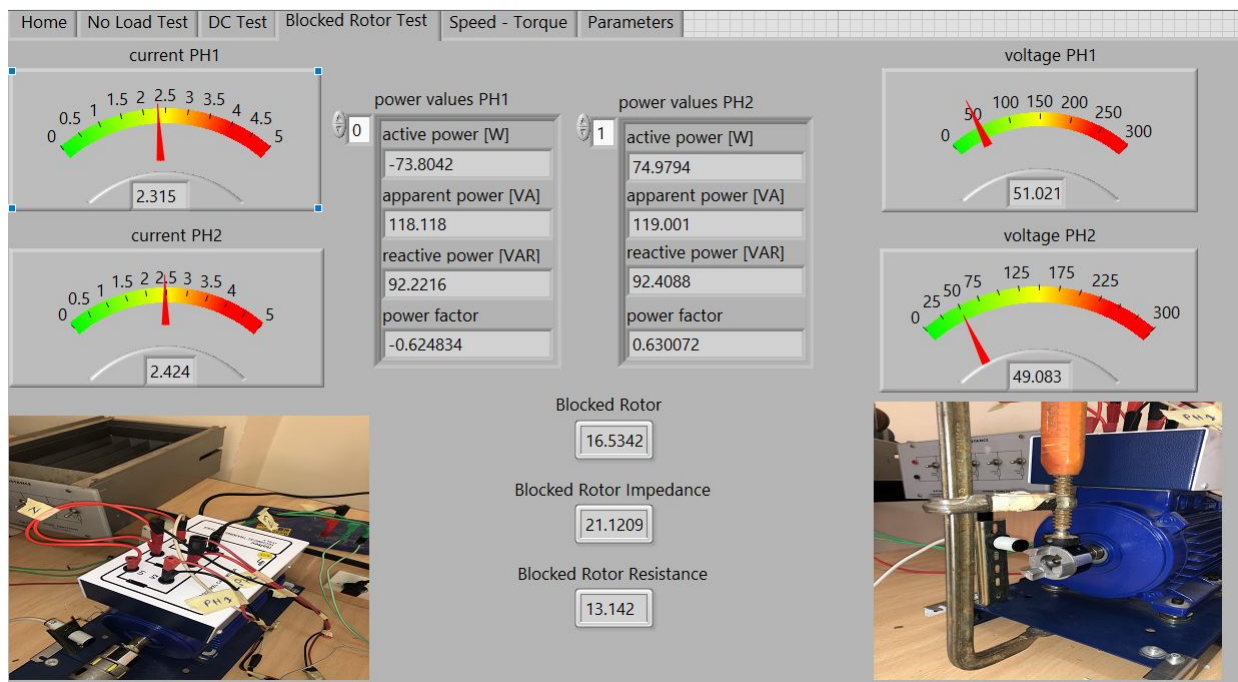


Figure 3.6: Blocked Rotor Tab during the Blocked Rotor Test

Similar to the No Load Test tab, the Blocked Rotor Test tab visualizes current, voltage, power, and other relevant measurements. However, in this test, the focus is on the blocked rotor condition. The voltage is slowly increased from 0V DC while monitoring the resulting current. The voltage is gradually adjusted until the current reaches the rated current of the motor, typically around 2.4 amps.

By analyzing the current and voltage graphs, researchers can determine the blocked rotor Reactance, blocked rotor Resistance, and blocked rotor Impedance. The values of blocked rotor Reactance, blocked rotor Resistance, and blocked rotor Impedance are smaller than the corresponding No Load values. This is primarily due to the size difference between the stator and rotor windings and the current flowing through them during the blocked rotor condition. In a three-phase AC motor, the stator windings are typically larger and more robust compared to the rotor windings.

When the motor is blocked or stalled, the rotor windings experience a higher current flow due to the increased torque required to overcome the resistance of the stationary rotor. This increased current causes a decrease in resistance and reactance values, resulting in smaller magnitudes for the blocked rotor Reactance, blocked rotor Resistance, and blocked rotor Impedance.

Therefore, the values of these parameters are expected to be smaller during the blocked rotor condition compared to the No Load condition. These values provide valuable insights into the motor's behavior under blocked rotor scenarios, aiding in the analysis of its starting capability, overload performance, and stray losses.

### 3.2.4 DC Test tab

The DC Test tab in the LabVIEW interface is dedicated to conducting the DC test on the three-phase AC motor. This test allows for the determination of an important parameter which is the winding resistance.

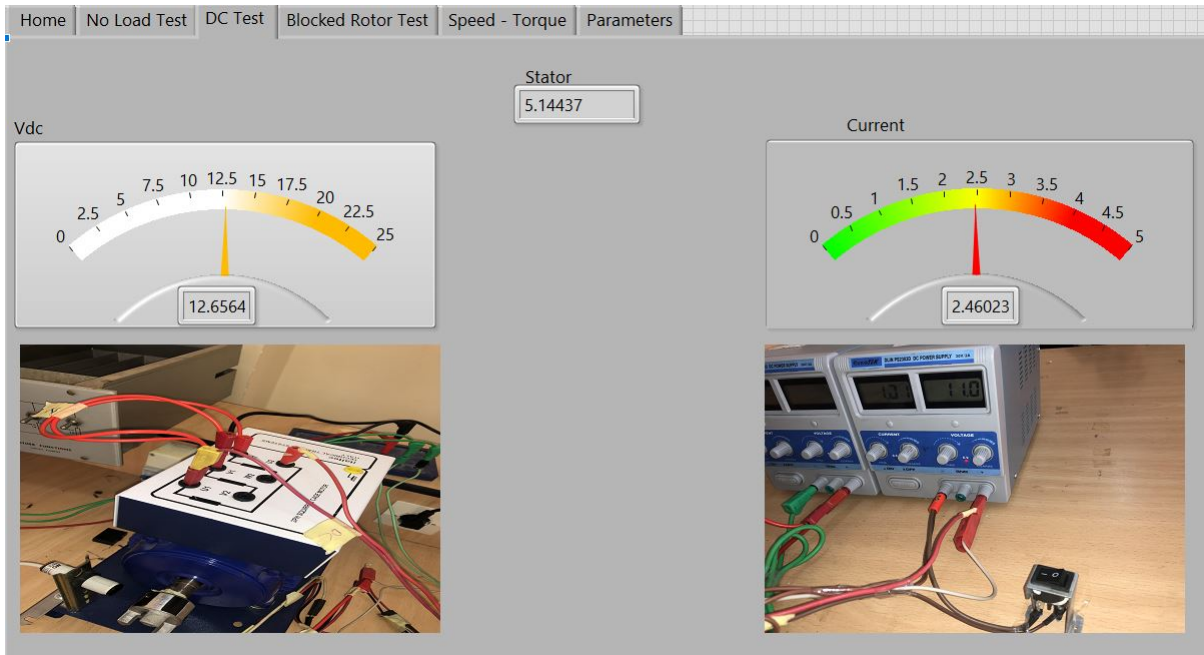


Figure 3.7: DC Tab during the DC Test

During the DC test, only one phase of the motor is connected to the DC power supply. The voltage is gradually increased until the current reaches the rated current of the motor. The DC Test tab provides a graphical representation of the voltage and current, allowing for realtime visualization and analysis of the test data. As the voltage is increased, the current rises until it reaches the rated current value. At this point, the measurements can be used to calculate the winding resistance using Ohm's law formula.

### 3.2.5 Speed-Torque tab

The Speed Torque tab within the LabVIEW interface is specifically designed for the characterization of the motor's speed and torque relationship under different load conditions. This tab provides a dynamic visualization of real-time speed and torque measurements, allowing researchers to analyze the motor's performance curve.

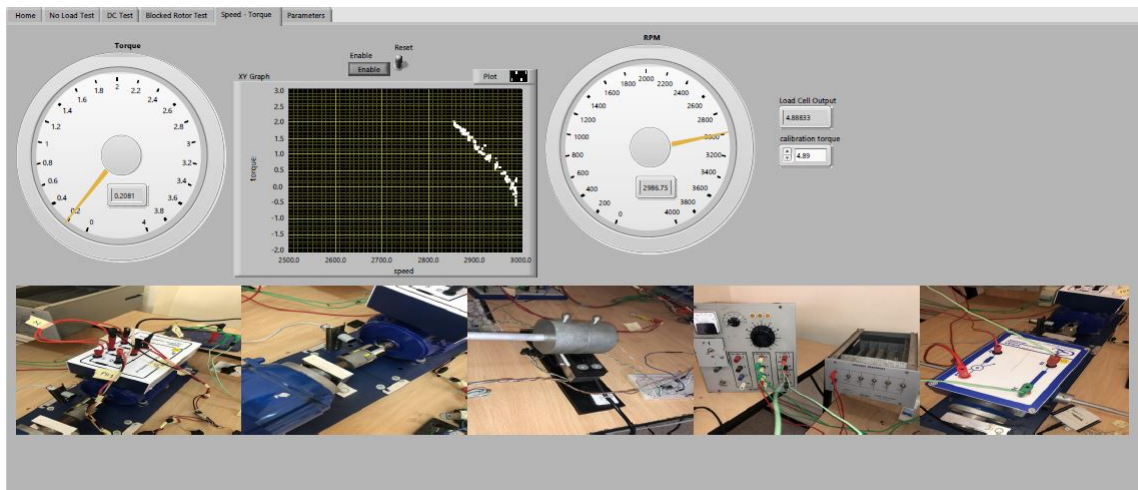


Figure 3.8: Speed-Torque Tab

Before conducting the speed torque characterization, the torque sensor is calibrated to ensure accurate data acquisition. Due to the amplification of the torque signal, calibration is essential for obtaining reliable measurements. The calibration process establishes a correlation between the sensor's output and the actual torque applied to the motor. Once the torque sensor is calibrated using the method explained in the torque measurement section of Chapter 2, researchers can observe the real-time speed and torque values on the Speed Torque tab while adjusting the mechanical load on the motor.

By altering the resistive load on the generator, researchers can effectively simulate different load conditions on the motor. As the load increases, the motor must generate additional torque to overcome the increased resistance and deliver the required power to the generator, all this without surpassing the motor rated current. As the load increases, the torque exerted by the motor increases, while the speed decreases. This inverse relationship between torque and speed is a fundamental characteristic of motor operation.

The Speed Torque tab provides a real-time visualization of the motor's speed and torque values as the load is adjusted. Researchers can observe how changes in the resistive load affect the motor's torque output and, consequently, its speed. This dynamic representation allows for the analysis of the motor's performance under varying load conditions. To visualize and analyze this relationship, a graph of torque as a function of speed is displayed on the tab. This graph provides a clear representation of how the motor's torque output varies with changes in speed under different load conditions.

By examining the shape of the torque-speed curve, researchers can determine the motor's maximum torque capability, its speed range, and its overall performance characteristics. The Speed Torque tab allows for real-time monitoring and analysis of the motor's speed and torque relationship, providing valuable insights into its performance capabilities. This information aids in optimizing motor operation, determining suitable load conditions, and evaluating the motor's suitability for specific applications.

### 3.2.6 The Parameters tab

The Final Parameters tab in the LabVIEW interface serves as the culmination of the motor parameter characterization process. In this tab, users can input the results obtained from the previous tests, such as the Stator Resistance, Load Reactance, Blocked Rotor Reactance, Blocked Rotor Resistance, and the NEMA type of the motor under evaluation. These inputs are utilized to derive important parameters of the induction motor equivalent circuit

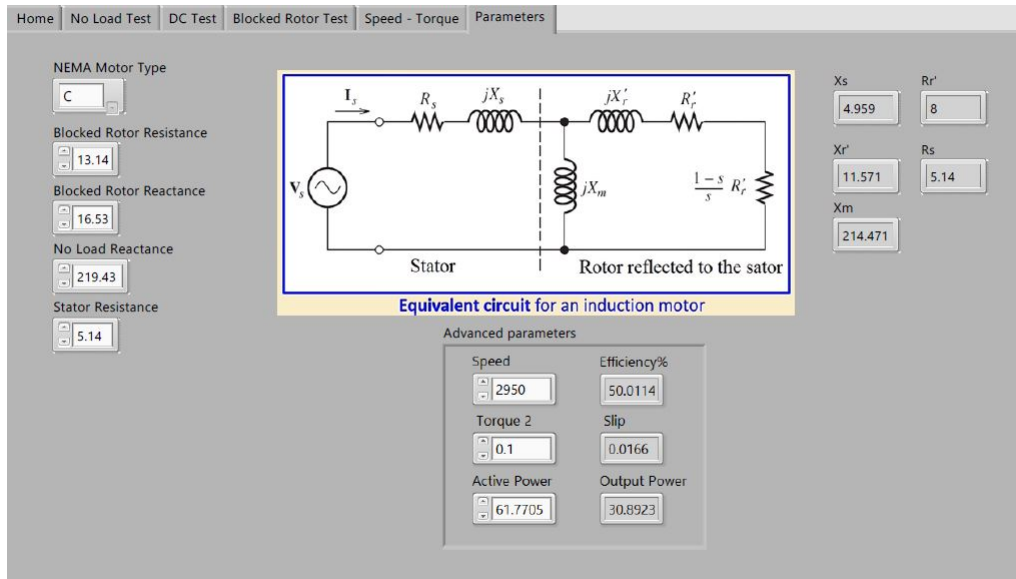


Figure 3.9: Parameters Tab

By inputting the relevant data, the Final Parameters tab provides a comprehensive analysis of the motor's performance. It enables the determination of key parameters such as the Stator Inductance, Magnetizing Reactance, and Leakage Reactance. These parameters contribute to a better understanding of the motor's electrical characteristics and aid in further analysis and design considerations.

Additionally, the Final Parameters tab offers advanced parameter calculations based on the speed, torque, and active power values obtained from the previous tests. By leveraging this information, it becomes possible to determine the motor's efficiency, slip, and output power. These parameters provide critical insights into the motor's operational efficiency, performance under different load conditions, and power output capabilities.

By utilizing this tab, researchers and engineers can evaluate the motor's characteristics against industry standards and specifications. This enables them to assess its performance, make informed decisions regarding motor selection and control strategies, and optimize its usage within specific applications.

### 3.3 Conclusion

In conclusion, Chapter 3 presented the developed platform and testing procedures for the evaluation of induction motors. The chapter began with an introduction to provide an overview of the purpose and objectives of the chapter. The developed platform, consisting of a tab control interface, was described in detail, highlighting its different sections and functionalities.

The Home tab provided a central point of navigation and access to various testing tabs. The No Load Test tab allowed for conducting tests under no-load conditions to measure parameters such as input power, stator current, and power factor. The Blocked Rotor Test tab facilitated tests performed under blocked rotor conditions to analyze parameters like locked rotor current and rotor impedance. The DC Test tab enabled measurements of parameters related to the DC operation of the motor.

The Speed-Torque tab provided a platform to assess the torque-speed characteristics of the induction motor. It allowed for controlling the speed and measuring the corresponding torque values. The Parameters tab served as a comprehensive reference for viewing and modifying motor parameters.

Furthermore, the chapter discussed the measurement methods and signal conditioning techniques employed in the testing procedures. Voltage measurement, current measurement, speed measurement, and torque measurement methods were explained, emphasizing their importance in accurately assessing motor performance.

The integration of LabVIEW and a Data Acquisition Device (DAQ) was also discussed, highlighting their roles in data acquisition, analysis, and control of the motor testing process.

Overall, Chapter 3 provided a detailed description of the developed platform and testing methodologies for the evaluation of induction motors. The platform and testing procedures presented in this chapter will serve as the foundation for the subsequent chapters, where the experimental results and analysis will be presented in order to achieve the objectives of this thesis.

# Conclusion

In this project, a semi-automatic test bench for the characterization of induction motors was successfully developed and implemented. The platform provides a user-friendly interface for accurate measurement and analysis of motor parameters, contributing to the efficient testing and optimization of motor performance.

Through a comprehensive literature review, we gained insights into the structure, functioning, and characteristics of induction motors. This knowledge guided the development of the test bench and ensured its compatibility with a wide range of motor types and applications.

The methods and measurement system section explored classical tests for induction motors, highlighting the importance of tests such as the locked rotor test, no-load test, and DC test. The measurement methods and signal conditioning techniques discussed enabled precise measurement of voltage, current, speed, and torque, ensuring reliable data acquisition.

The developed platform description and testing section presented a tab control interface that allows users to perform various tests, including the no-load test, blocked rotor test, DC test, and speed-torque analysis. The Parameters tab facilitates comprehensive motor parameterization, enabling users to evaluate motor performance and efficiency accurately.

While the semi-automatic test bench has proven to be a valuable tool for induction motor characterization, there are several avenues for future improvement and expansion:

- **Integration of additional tests:** The test bench could be enhanced by incorporating further tests, such as temperature rise tests or efficiency measurements. This would provide a more comprehensive analysis of motor performance.
- **Automation and remote operation:** The platform could be further developed to enable automation of test procedures and remote operation. This would reduce human error and allow for testing in remote or inaccessible locations.
- **Validation and calibration:** Future work should involve rigorous validation and calibration of the test bench to ensure its accuracy and reliability. Comparison with standard reference motors or certified testing facilities would help establish confidence in the obtained results.



# Bibliography

- [1] B. S. Guru and H. R. Hiziroglu, *Electric Machinery and Transformers*. Oxford University Press, 2001.
- [2] P. C. Sen, *Principles of Electric Machines and Power Electronics*. Wiley, 2013.
- [3] R. Krishnan, *Electric Motor Drives: Modeling, Analysis, and Control*, Wiley-IEEE Press, 2001.
- [4] A. Hand, *Electric Motor Maintenance and Troubleshooting*, Fairmont Press, 2008.
- [5] F. Mansor, *Induction Motors: Construction, Principle of Operation, Power and Torque Calculations, Characteristics and Speed Control*, Lambert Academic Publishing, 2016.
- [6] A. Hughes and B. Drury, *Electric Motors and Drives: Fundamentals, Types and Applications*, Newnes, 2013.
- [7] Filizadeh and S. Shaahin, *Electric Machines and Drives: Principles, Control, Modeling, and Simulation*, CRC Press, 2017.
- [8] E. Ramprasath and P. Manojkumar, *Modelling and Analysis of Induction Motor Using Labview*, LAP Lambert Academic Publishing, 2019.
- [9] IEEE Standards Association, "IEEE Standard Test Procedure for Polyphase Induction Motors and Generators," IEEE Std 112-2004.
- [10] R. McElven and M. Melfi, Locked Rotor Test Methods for Induction Motors Investigated, in 2015 IEEE Industry Applications Society Annual Meeting, Addison, TX, USA, 2015, pp. 1-8. doi: 10.1109/IAS.2015.7435098.
- [11] C. D. Pitis, Performing Locked Rotor Test on Squirrel Cage Motors, 2015. [Online]. Available: [https://www.researchgate.net/publication/280558869\\_PERFORMING\\_LOCKED\\_ROTOR\\_TEST\\_ON\\_SQUIRREL\\_CAGE\\_MOTORS](https://www.researchgate.net/publication/280558869_PERFORMING_LOCKED_ROTOR_TEST_ON_SQUIRREL_CAGE_MOTORS). [Accessed: May 02, 2023].
- [12] J. A. Melkebeek, *Electrical Machines and Drives: Fundamentals and Advanced Modelling*, Springer International Publishing, 2018.
- [13] I. Boldea and S. A. Nasar, *The Induction Machine Handbook*. 2001.
- [14] G. W. McPherson, *An Introduction to Electrical Machines and Transformers*. 1981. [Online]. Available: <http://ci.nii.ac.jp/ncid/BA0688067X>. [Accessed: May 4, 2023].

- [15] Journal of Visualized Experiments (JoVE), AC Induction Motor Characterization. [Online]. Available: <https://www.jove.com/v/10150/ac-induction-motor-characterization>. [Accessed: May 4, 2023].
- [16] P. Horowitz and W. Hill, The Art of Electronics, 3rd ed., Cambridge University Press, 2015.
- [17] Energia Zero, "Arduino 25V Voltage Sensor Module," in Energia Zero Arduino Sensori, Available: [http://www.energiazero.org/arduino\\_sensori/arduino%2025v%20voltage%20sensor%20module.pdf](http://www.energiazero.org/arduino_sensori/arduino%2025v%20voltage%20sensor%20module.pdf), Accessed: May 25, 2023.
- [18] S. W. Smith, The Scientist and Engineer's Guide to Digital Signal Processing, 2nd ed. San Diego, CA, USA: California Technical Pub., 1999.
- [19] Allegro Microsystems. (n.d.). ACS712 Datasheet. [Online]. Available: <https://www.alldatasheet.com/datasheet-pdf/pdf/168326/ALLEGRO/ACS712.html>. Accessed on: May 25th, 2023.
- [20] S. L. Herman, Industrial Motor Control, Cengage Learning, 2010.
- [21] Omron, E3F1 Photoelectric Sensor, Compact M18 Housing Datasheet. [Online]. Available: [https://assets.omron.eu/downloads/datasheet/en/v3/e94e\\_e3f1\\_photoelectric\\_sensor\\_compact\\_m18\\_housing\\_datasheet\\_en.pdf](https://assets.omron.eu/downloads/datasheet/en/v3/e94e_e3f1_photoelectric_sensor_compact_m18_housing_datasheet_en.pdf). [Accessed: May 25, 2023].
- [22] A. Farley, "Design and Implementation of a Small Electric Motor Dynamometer for Mechanical Engineering Undergraduate Laboratory," Graduate Theses and Dissertations, 2012. [Online]. Available: <https://scholarworks.uark.edu/etd/336>. [Accessed: May 25, 2023].
- [23] B. Amin, Induction Motors: Analysis and Torque Control. Springer, 2001.
- [24] Datasheet 3134 - Micro Load Cell (0-20kg) - CZL635, Gotronic, [Online]. Available: <https://www.gotronic.fr/pj-460.pdf>. [Accessed: May 26, 2023].
- [25] Texas Instruments, INA101 Datasheet, Literature Number GPN/INA101, August 2001. [Online]. Available: <https://www.ti.com/lit/gpn/INA101>. [Accessed: May 25, 2023].
- [26] J. Jerome, Virtual Instruments using LabVIEW, Academia.edu. [Online]. Available: [https://www.academia.edu/9455052/Virtual\\_Instruments\\_using\\_LabView](https://www.academia.edu/9455052/Virtual_Instruments_using_LabView). [Accessed: May 20, 2023].
- [27] National Instruments. (n.d.). National Instruments [Online]. Available: <https://www.ni.com/en-lb.html>. [Accessed: May 20, 2023].
- [28] USB-6008/6009 User Guide, SFU Chemical Instrumentation Facility, [Online]. Available: [https://c7076-control.chem.sfu.ca/interlock\\_monitoring\\_system\\_resources/usb6008.pdf](https://c7076-control.chem.sfu.ca/interlock_monitoring_system_resources/usb6008.pdf). [Accessed: May 20, 2023].

# Appendix

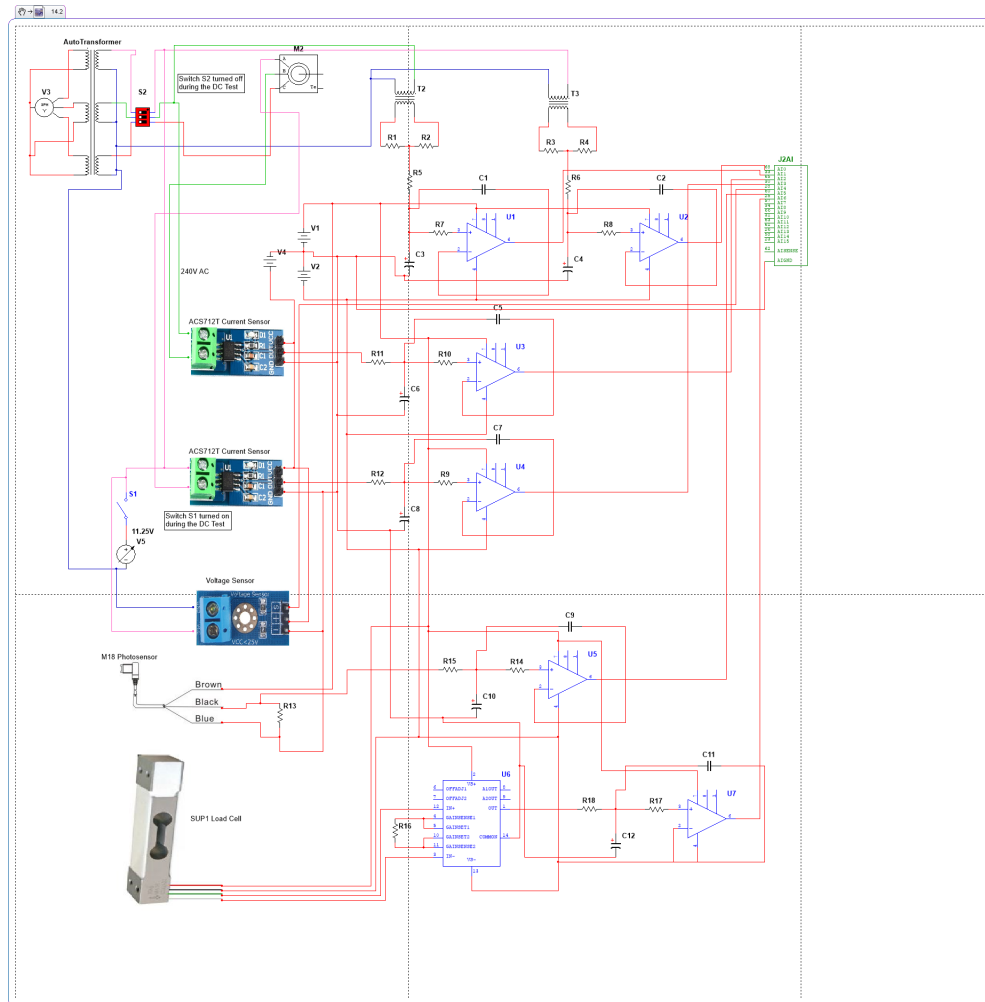


Fig A1: Complete Diagram of the Testing Circuit

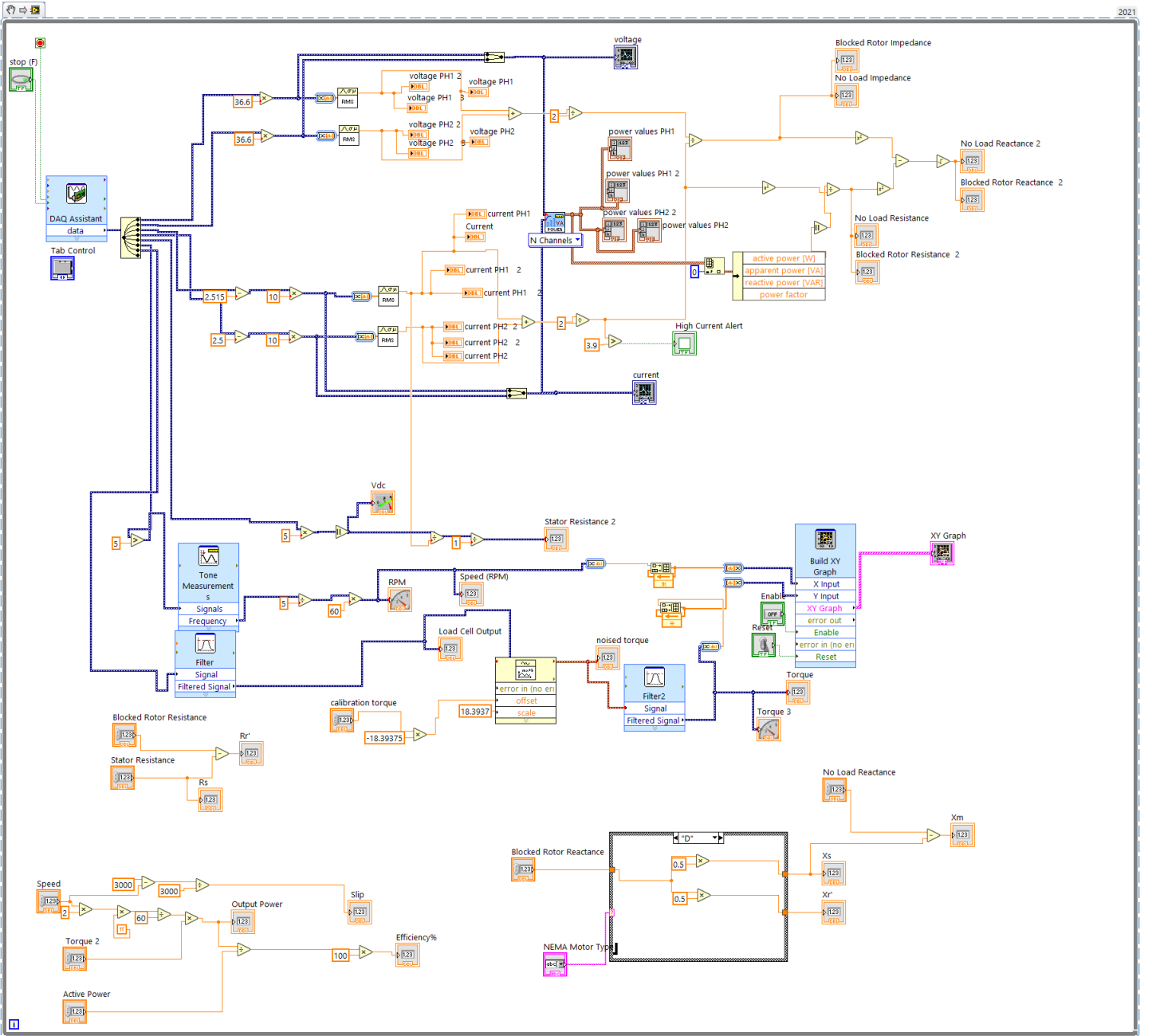


Fig A2: Complete Diagram of the Labview Code